Novel Broadband Calibration Method of Current Shunts Based on VNA

Article *in* IEEE Transactions on Instrumentation and Measurement · July 2018

DOI: 10.1109/TIM.2018.2855499

Mohamed Ouameur
Laboratoire national de métrologie et d'essais LNE, France, Paris

François Ziade
Laboratoire National de Métrologie et d'Essais

Novel Broadband Calibration Method of Current Shunts Based on VNA

Mohamed Ouameur, François Ziade, and Yann Le Bihan

***Abstract*— Usually high wideband ac current and harmonics measurements are accurately achieved in industry and laboratories by using high accuracy shunts or standard shunts. For particular applications, such as power and transient measurements, it is mandatory to evaluate the shunt impedance phase and magnitude according to the frequency bandwidth of interest before to measure the current with such sensors. High electrical current shunt beyond 1 A is calibrated in magnitude up to 100 kHz and in phase angle up to 200 kHz only by a few National Metrology Institutes. The existing traceable measurement methods to characterize these sensors are limited in frequency to 100 kHz, with expanded uncertainties of the ac–dc difference (magnitude) and the phase angle of more than 5×10^{-6} and 62 μrad at 100 kHz, respectively. A new traceable calibration method to measure and characterize current shunts at high frequencies is presented in this paper. This measurement method is based on the use of a vector network analyzer. The measurements are presented up to 60 MHz, but theoretically, the presented method does not exhibit a specific frequency limitation. Only the characteristics of the shunt under study can impose limitation in practice. While uncertainties are higher than those provided by the existing methods, the method presented in this paper is the only method able to perform in one step a broadband and simultaneous measurement of the magnitude and phase of current shunts up to few megahertz with acceptable uncertainties.**

***Index Terms*— AC–DC difference, calibration method, current measurement, current shunt, phase angle, uncertainty, vector network analyzer (VNA), wideband measurements.**

I. Introduction

INCREASINGLY, it is necessary to measure high levels of currents on a wide frequency bandwidth because of high-current events such as short-circuit transient and impulse currents occurring in many applications such as the development of electric vehicles, and the production, transport, and distribution of energy. This calls for the characterization of wideband current sensors up to the megahertz frequency range. Unfortunately, for high levels of currents, the traceability and the calibration methods of such devices are not available in these extreme frequencies. Up to 1 MHz, the existing methods are designed to measure low current levels (up to 1 A) [1]. For high current levels (beyond 1 A), the measurement frequency bandwidth is limited to 100 kHz [2].

The frequency variation of the impedance Z_{shunt} of a shunt is characterized by [3] as follows.

1) The variation in frequency of the impedance magnitude compared to its dc value (ac–dc difference δ), generally given as

$$\delta = \frac{|Z_{\text{shunt}}| - R_{\text{dc}}}{R_{\text{dc}}} \tag{1}$$

where R_{dc} is the direct current (dc) resistance of the current shunt.

2) The impedance phase angle of the current shunt, defined as [4]

$$\phi = \arctan\left(\frac{\Im[Z_{\text{shunt}}]}{\Re[Z_{\text{shunt}}]}\right) \tag{2}$$

where $\Im\ [Z_{\text{shunt}}]$ is the imaginary part of the shunt impedance and $\Re\ [Z_{\text{shunt}}]$ is the real part of the shunt impedance.

Following [3], it is noted that the definition of ac–dc difference δ given in (1) is equivalent to the one recommended by the consultative committee for electricity and magnetism of the International Committee for Weights and Measures (CIPM). The definition given in (1) has been used since the method presented in this paper is based on the impedance modeling of current shunts which are calibrated.

II. Existing Calibration Methods of Shunts

Metrologically, the existing calibration methods deliver very good results up to typically 100 kHz and 1 A [5]–[8] but only one parameter is measured: either the ac–dc difference or the phase angle. We can briefly classify the existing shunt measurement methods in the following categories.

A. Direct Comparison Method

The principle of this method is based on the direct comparison of voltages measured between terminals of two series connected shunts: one ac shunt standard and one ac shunt under test being calibrated. The range of voltages is identical for both devices during the calibration process.

This method has been used to measure the absolute phase angle errors between 100 and 300 mA up to 1 MHz of current shunts based on a "cage" topology of resistors [1]. To assess the phase angle error, a phase comparator has been

Manuscript received December 19, 2017; revised April 10, 2018; accepted June 19, 2018. The Associate Editor coordinating the review process was Dr. Thomas Lipe. *(Corresponding author: François Ziade.)*

M. Ouameur is with the Laboratoire National deMétrologie et d'Essais, 78197 Trappes, France, and also with GeePs, Laboratoire Génie Electrique et Electronique de Paris, 91192 Gif-sur-Yvette, France (e-mail: francois.ziade@lne.fr).

F. Ziade is with the Laboratoire National deMétrologie et d'Essais, 78197 Trappes, France.

Y. L. Bihan is with GeePs, Laboratoire Génie Electrique et Electronique de Paris, 91192 Gif-sur-Yvette, France (e-mail: yann.le-bihan@geeps.centralesupelec.fr).

Color versions of one or more of the figures in this paper are available online at http://ieeexplore.ieee.org.

Digital Object Identifier 10.1109/TIM.2018.2855499

developed based on [1], [4], [6], [9], and [10]. The two current shunts to be compared are connected in series using a current T-connector in a measurement setup composed of an ac current source and two 2-channel digitizers. The expanded uncertainty ($k = 2$) of the phase angle error is ± 200 μrad at 1 MHz.

A wideband phase comparator has been developed in order to perform phase angle measurements with higher levels of current [5] from 2 to 100 A and for frequencies from 500 Hz to 100 kHz [6]. The expanded uncertainty ($k = 2$) of the phase angle error is ± 50 μrad at 100 kHz for levels of current up to 10 A.

An automated measuring system has been developed to assess the impedance magnitude deviation from dc of ac–dc current transfer standards. The principle is based on the connection of the two thermal current converters. The difference between the output of the current converters and the back-off voltages are measured by nano-voltmeters [11]. The uncertainty of ac–dc difference is estimated less than ± 50 mA/A for currents up to 30 mA and frequencies up to 100 kHz.

Generally, the direct comparison method suffers from the existence of a reversal error occurring when the relative positions of the two current shunts are reversed [12]. Accordingly, one approach has been developed and applied to compare current outputs from an ac shunt standard with a current probe [12]. The ac–dc difference of "cage" current shunts has been found to be less than 10 ppm up to 100 kHz without giving an estimated uncertainty.

B. Thermal Transfer Method

The thermal transfer method is commonly used in the National Metrology Institutes (NMIs) to measure alternating voltage or ac current up to the megahertz range. The measurement method, based on a thermocouple, measures the continuous value of the electric quantity (current or voltage) which causes the same heating effect generated by the alternating value to be assessed.

In 2011, results of various existing shunts have been published [6] on the basis of the thermal transfer method. The shunts used for the ac–dc current transfer are of planar multijunction thermal converters type (PMJTC) [13], [14]. The PMJTC type is used to obtain the lowest uncertainties of the measurement, but these are not easily available commercially. The expanded uncertainty of the ac–dc difference is preliminarily estimated to be 9 μA/A from 10 Hz to 100 kHz for current levels ranging from 30 mA to 10 A.

A resonant method has been developed to calibrate current probes at a current level of 10 A and frequencies up to 1 MHz [15]. In this method, a 1-Ω resistor is characterized by the thermal transfer method up to 100 kHz and using a VNA traceable to International System of units (SI) in the megahertz range [16]. The reported uncertainties are of 2% at 1 MHz.

C. Potentiometer method

Another measurement method has been developed to characterize the phase angle of current shunts from 40 Hz to 200 kHz [9]. This approach is based on the use of 3-D multijunction thermal converters (TPC), precision amplifiers, and a specialized measurement algorithm [17]. The uncertainties of the phase angle are 141 μrad from 100 mA to 20 A, at frequencies from 40 Hz to 200 kHz.

At current levels of 10 A and 100 kHz, the existing measurement methods previously published by different NMIs for measuring the phase angle, and ac–dc difference exhibits an expanded uncertainty ($k = 2$) of at least 62 μrad and 6 ppm, respectively. Currently, no existing method enables to measure simultaneously the ac–dc difference and the phase angle. These approaches are limited to 200 kHz for current levels exceeding 10 A. Furthermore, the traceability to the SI for most methods is not completely achieved beyond 100 kHz.

In this paper, we present a new measurement method adapted for characterizing simultaneously the ac–dc difference and phase angle of current shunts up to a few megahertz. In what follows we will present successively the method, the uncertainty calculation, and the measurement results.

III. Shunt Calibration Method Using AVNA

The proposed calibration method is based on a vector network analyzer (VNA) which has some attractive features such as low sweep time, broad frequency bandwidth, and capability of measuring complex S-parameters. The proposed method requires the measurement of S-parameters from the lowest available frequency (below a few tens of kilohertz) up to a few tens of megahertz. Practically, an Agilent E5071C with a frequency bandwidth ranging from 9 kHz to 4.5 GHz is used for the measurements. The S-parameter uncertainty of a VNA is impacted by systematic error terms: directivity, source match, reflection tracking, transmission tracking, and load match [18]. Before using a VNA, a calibration method is mandatory to remove the systematic errors. The unknown thru method [19] is used to calibrate the VNA from 9 kHz to 100 MHz. The unknown thru calibration method is based on the use of three impedance standards (open, short, and 50-Ω loads) and an additional unknown thru connection. This latter is a transmission line for which the characteristics are determined during the calibration process. The traceability of the VNA measurements is established through the precise knowledge of the 50-Ω impedance standard according to the frequency [16] and using a type N calibration kit completely calculable from dc to 1 GHz [2]. Once the VNA is calibrated, the shunt is simply connected to the VNA and its S-matrix measured on the frequency bandwidth of interest. The system for measuring the S-parameters of a two-port shunt is shown in Fig. 1.

Generally, the impedance Z_{shunt} of a two-port shunt is defined by its transmission impedance Z_{21} from port 1 (current input) to port 2 (voltage output). Therefore, this impedance is calculated from the S-parameter values measured with a VNA. The impedance of the 50-Ω load standard used during the VNA calibration is completely calculable and traceable to SI. The variation of real and imaginary parts of the load standard impedance is very low. It follows that S-parameters measurements of a shunt can be accurately normalized to the

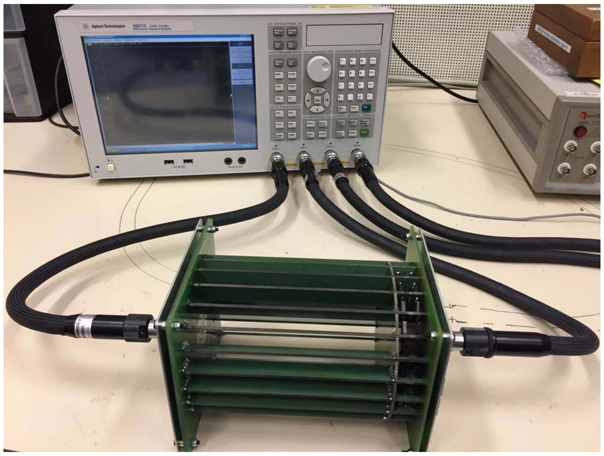

Fig. 1. Measurement of the S-parameters of an ac coaxial shunt based on a "cage" geometry using a VNA.

characteristic impedance Z_0 equal to 50 Ω. After calibration of the VNA, the reference planes of S-parameters measurement correspond to current and voltage connectors of the current shunt. Hence, S-parameters that are determined this way are intrinsic characteristics of the shunt: they characterize the shunt itself independently of the VNA input impedance. Finally, values of the transfer impedance Z_{21}, and consequently, values of the shunt's model determined using the S-parameters are independent of the VNA input impedance. Using the method presented in this paper, shunts are characterized as four-terminal impedance and it is not required to consider any loading errors. The transfer impedance Z_{21} (Z_{shunt}) is expressed from S-parameters and the characteristic impedance Z_0 is equal to 50 Ω [20]

$$Z_{21} = Z_0 \frac{2\ S_{21}}{(1 - S_{11})(1 - S_{22}) - S_{12}S_{21}}. \tag{3}$$

The real and imaginary parts of S-parameters of the current shunt are measured and stored for data postprocessing. For the calculations, the following notations are used:

$$\begin{cases} S_{11} = \alpha_{11} + j\beta_{11} \\ S_{12} = \alpha_{12} + j\beta_{12} \\ S_{21} = \alpha_{21} + j\beta_{21} \\ S_{22} = \alpha_{22} + j\beta_{22} \end{cases} \tag{4}$$

The real and imaginary parts of the measured shunt impedance Z_{21} can be expressed by

$$\begin{cases} \Re_{\text{mes}}[Z_{21}] = 2\ Z_0\, \dfrac{\alpha_{21}K_1 + \beta_{21}K_2}{K_1^2 + K_2^2} \\ \Im_{\text{mes}}[Z_{21}] = 2\ Z_0\, \dfrac{\beta_{21}K_1 - \alpha_{21}K_2}{K_1^2 + K_2^2} \end{cases} \tag{5}$$

where

$$K_1 = 1 - \alpha_{11} - \alpha_{22} + \alpha_{11}\alpha_{22} - \beta_{11}\beta_{22} - \alpha_{12}\alpha_{21} + \beta_{12}\beta_{21} \tag{6}$$

$$K_2 = \alpha_{11}\beta_{22} + \alpha_{22}\beta_{11} - \beta_{11} - \beta_{22} - \alpha_{12}\beta_{21} - \alpha_{21}\beta_{12}. \tag{7}$$

The VNA has a standard output impedance of 50 Ω, whereas the impedance of the current shunt is generally observed to

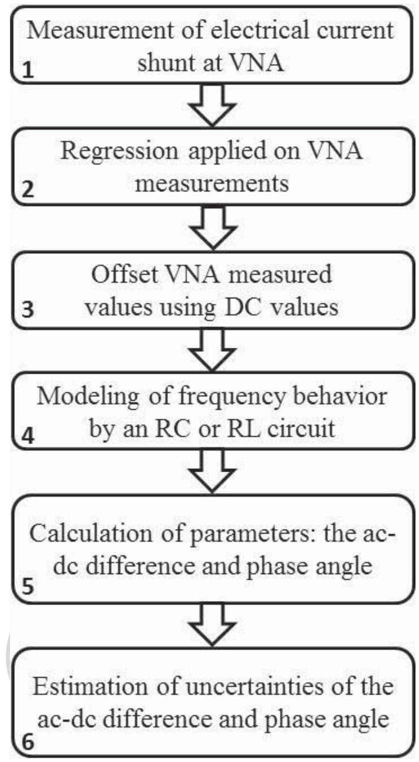

Fig. 2. Steps of the proposed measurement method.

be less than 2 Ω. For instance, the device under test (DUT) presented in Fig. 1 is an ac coaxial current shunt of 10 A based on the cage geometry with a dc resistance nominal value of 0.08 Ω [4]. This impedance deviation between the DUT and VNA produces noise and low accuracy in measurements. As it stands, VNA measurement data cannot be used directly to assess shunt parameters.

The purpose of this new measurement method is to prevent the effect of the mismatch between the shunt and the VNA output impedance by applying a regression on VNA measurements data and providing modeling of the shunt. The description of the method is detailed as follows (Fig. 2).

Step 1: The shunt to be calibrated is measured with a VNA. An average of 10 measurements is calculated to reduce the connectors' repeatability error.

Step 2: A polynomial regression is applied to the VNA measurements. The influence of the measurement noise is reduced using a regression: linear for the imaginary part and polynomial of degree two for the real part. The polynomial and linear regression have been validated by using Pearson's chi-squared test.

*Step 3:*The regressed curves are shifted to match the dc value of the shunt. The use of the VNA is indeed mainly aimed at evaluating the variation in frequency, because the dc value of the shunt cannot be measured directly and exactly with a VNA and is instead measured with a Digital Multimeter standard calibrated.

Step 4: A model of the measured shunt is obtained by calculating the values of an equivalent circuit of the shunt constituted of either an *RL* circuit (a resistor in series with

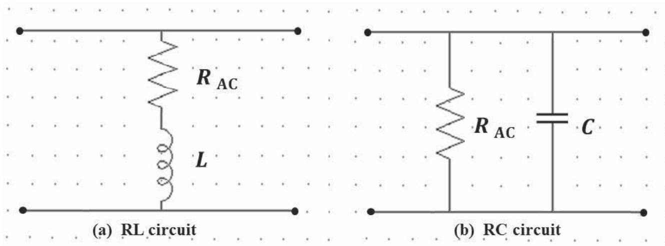

Fig. 3. Equivalent circuit of the shunt considered. (a) *RL* circuit. (b) *RC* circuit.

an inductor) or an *RC* circuit (a resistor in parallel with a capacitor) (Fig. 3). The choice of the equivalent circuit configuration is based on the sign of the imaginary part of the measured shunt impedance: for instance, if the imaginary part of the shunt impedance is negative, a circuit model (R, C) is applied.

Step 5: The determination of the electrical equivalent model allows calculating the values of the ac–dc difference and phase angle with low associated uncertainties.

Step 6: Uncertainty calculation associated with this measurement method is finally calculated. The calculation is detailed in Section IV.

The shunt can be calibrated between dc and a few tens of megahertz depending on its frequency variation. In this paper, the frequency limit for the measurements does not exceed 60 MHz for which the wavelength λ is approximately 5 m. The shunt's length considered in this paper is less than 30 cm. In a general way, the transmission line theory could be applied to calculate Z_{21} but as shown in Section V, a simple (R, L) or (R, C) equivalent circuits of a shunt is appropriate and accurate to model Z_{21} because structures and values of the modeling are directly determined from measurements. Consequently, potential transmission line effects are taken into account in this case.

In the case of (R, L) circuit, the shunt inductance is composed of the two following: internal and external inductances. In a general way, internal inductance is dependent on skin effects, but in the shunts considered in this paper, the external inductance is the most preponderant inductance and is independent of the frequency. The validity of this approximation is observed in the imaginary part measured: the reactance is linear according to the frequency range of interest. The linear regression applied to the reactance part has been validated by the statistical Pearson's chi-squared test (Figs. 5 and 7). In this particular case, the skin effect can be considered as negligible on the reactive part of Z_{shunt}.

In practice, the frequency limitations of the method are linked to current shunt:

1) presenting a simple equivalent electrical model (*RL* or *RC*);
2) having a temperature-independent frequency variation;
3) characterized by a negligible skin effect on the reactive part of Z_{shunt} in the frequency range of interest.

In a general way, the resistance part of a shunt is subject to variation mainly due to resonance and skin effect at high frequencies. Different shunts considered in this paper have a frequency variation that can be approximated using a second-degree polynomial regression. This latter has been validated by performing the statistical Pearson's chi-squared test: the regression describes appropriately the measurements taking into account the standard deviation.

IV. Uncertainty Calculation

The uncertainty evaluation of ac–dc difference and phase angle has been achieved according to the "evaluation of measurement data—a guide to the expression of uncertainty in measurement" (GUM) [21]. The experimental measurement values are considered to calculate the standard deviation of each variable from the equivalent electrical model and finally to evaluate uncertainties on ac–dc difference and phase angle parameters. The presented method involves nonlinear measurement functions for the measurands: ac–dc difference and phase angle. The law of propagation of uncertainty based on a first-order Taylor series expansion can leads to incorrect standard uncertainties of the results when nonlinear measurement functions are involved in the calculation. Indeed, if the nonlinearity of functions is significant, higher order terms in the Taylor series expansion must be included in the expression of the combined standard uncertainty. In this paper, it has been verified that the nonlinearity does not affect significantly the combined uncertainties of the two measurands (ac–dc difference and phase angle) calculated with the first-order Taylor series expansion. This verification has been performed according to the method described in GUM supplement 1 [22]: it consists of applying the Monte Carlo method using one million samples to calculate the distribution of the measurand. Once the distribution is obtained, the mean, the standard deviation, and the 95% confidence interval can be calculated and compared to the classical law of propagation of uncertainty results. The calculation has been performed to the following frequencies 100 kHz, 1 MHz, 10 MHz, and 40 MHz and compared to the GUM classical results. The normal distribution obtained by the Monte Carlo method validates the use of a coverage factor of 2. The difference between the two approaches is negligible and demonstrates that the first-order Taylor series approximation can be applied to calculate the combined standard uncertainty presented in this novel broadband calibration method of current shunts based on VNA. Considering the number of frequency measurement points and the use of a polynomial regression, the Monte Carlo method is time-consuming which justifies the implementation of the classical GUM approach.

Different types A and B uncertainty contributions considered in our calculation are the following.

1) Repeatability condition of measurement (type A):
   a) The VNA has been calibrated one time and ten measurements have been performed in a very short time by connecting and disconnecting connectors between each measurement.
2) The intermediate precision condition of measurement (type A):

a) The VNA has been calibrated one time each day for three consecutive days and measurements have been performed after each calibration.

3) Reproducibility condition of measurement (type A):

a) The VNA has been calibrated and measurements performed by two different operators.

b) Two different measurements have been performed using two different VNAs (change in the measuring systems) and cables.

c) Two different calibration kits have been used to calibrate and perform two different sets of measurements

4) Accuracy of the standards modeling (type B).
5) Correlation of S-parameters (type B).
6) Errors related to the interpolation process (type B).
7) Errors of the shunt modeling (type B).

A. RL Circuit

As explained before, if a current shunt exhibits a predominant inductive behavior in the frequency range of interest, its complex impedance can be described simply by a resistor–inductor series circuit (*RL* circuit)

$$Z_{21} = R_{\mathrm{ac}} + jL\omega \tag{8}$$

where R_{ac} and L are, respectively, the ac resistor and inductor of the considered *RL* circuit. R_{ac} and L are given as

$$\begin{cases} R_{\mathrm{ac}} = \Re_{\mathrm{reg}}[Z_{21}] \\ L = \dfrac{\Im_{\mathrm{reg}}[Z_{21}]}{\omega} \end{cases} \tag{9}$$

where $\Im_{\mathrm{reg}}[Z_{21}]$ and $\Re_{\mathrm{reg}}[Z_{21}]$ result from the linear regression of the imaginary part and from the polynomial regression of degree 2 of the real part of the shunt impedance, respectively. The real and imaginary parts can be expressed in terms of the regression coefficients and the frequency as

$$\begin{cases} \Re_{\mathrm{reg}}[Z_{21}] = a_0 + a_1 f + a_2 f^2 \\ \Im_{\mathrm{reg}}[Z_{21}] = b_1 f \end{cases} \tag{10}$$

where a_i and b_1 are, respectively, the polynomial regression coefficients of the real part and linear regression coefficient of the imaginary part, and f is the frequency.

The polynomial degrees are chosen using the frequency behavior of the shunt to be characterized. Noting that in dc, the real and imaginary parts are equal, respectively, to the measured value by a digital multimeter ($R_{\mathrm{dc}} = a_0$) and to zero.

Finally, the expressions in (10) permit to calculate the regression uncertainties using uncertainty propagation, such as

$$\begin{aligned} u^2(\mathrm{R}_{\mathrm{reg}}[Z_{21}]) &= \left(\frac{\partial \mathrm{R}_{\mathrm{reg}}[Z_{21}]}{\partial a_0}\right)^2 u^2(a_0) + \left(\frac{\partial \mathrm{R}_{\mathrm{reg}}[Z_{21}]}{\partial a_1}\right)^2 u^2(a_1) \\ &\quad + \left(\frac{\partial \mathrm{R}_{\mathrm{reg}}[Z_{21}]}{\partial a_2}\right)^2 u^2(a_2) + \left(\frac{\partial \mathrm{R}_{\mathrm{reg}}[Z_{21}]}{\partial f}\right)^2 u^2(f) \end{aligned} \tag{11}$$

where $u(x)$ is the standard uncertainty of the parameter x.

The uncertainty of the frequency parameter is negligible compared to the other components of uncertainty.

Consequently, (11) can be expressed as

$$u^2(\Re_{\mathrm{reg}}[Z_{21}]) = u^2(a_0) + f^2 u^2(a_1) + f^4 u^2(a_2). \tag{12}$$

For the imaginary part, from (10), we can express its uncertainty as

$$u^2(\Im_{\mathrm{reg}}[Z_{21}]) = \left(\frac{\partial \Im_{\mathrm{reg}}[Z_{21}]}{\partial b_1}\right)^2 u^2(b_1) = f^2 u^2(b_1). \tag{13}$$

The uncertainty of the regression coefficients is estimated by a standard error (square root of a variance) [**?**]. These uncertainties depend on the measurement uncertainties of the real $u(R_{\mathrm{mes}})$ and imaginary $u(I_{\mathrm{mes}})$ parts of the measured impedance Z_{21}. $u(R_{\mathrm{mes}})$ and $u(I_{\mathrm{mes}})$ are propagated from the uncertainty of the S-parameters measured with a VNA.

The measurement uncertainties of the real $u(R_{\mathrm{mes}})$ and imaginary u(I_{mes}) parts of Z_{21} are calculated by

$$u^2(\Re_{\mathrm{mes}}[Z_{21}]) = \sum_{i=1}^{2}\sum_{j=1}^{2} \begin{pmatrix} \left(\frac{\partial \Re_{\mathrm{mes}}[Z_{21}]}{\partial \alpha_{ij}}\right)^2 u^2(\alpha_{ij}) \\ + \left(\frac{\partial \Re_{\mathrm{mes}}[Z_{21}]}{\partial \beta_{ij}}\right)^2 u^2(\beta_{ij}) \end{pmatrix} \tag{14}$$

$$u^2(\Im_{\mathrm{mes}}[Z_{21}]) = \sum_{i=1}^{2}\sum_{j=1}^{2} \begin{pmatrix} \left(\frac{\partial \Im_{\mathrm{mes}}[Z_{21}]}{\partial \alpha_{ij}}\right)^2 u^2(\alpha_{ij}) \\ + \left(\frac{\partial \Im_{\mathrm{mes}}[Z_{21}]}{\partial \beta_{ij}}\right)^2 u^2(\beta_{ij}) \end{pmatrix} \tag{15}$$

where $u(\alpha_{ij})$ and $u(\beta_{ij})$ are the standard uncertainty of real and imaginary parts of S-parameters measured. These uncertainties are those obtained using a calibration kit developed at LNE to calibrate the VNA: standard uncertainties of u(α ij) and u(β ij) ranges from 5.10-5 to 5.10-2 and 8.10-5 to 0.25 respectively. The covariance matrices between real and imaginary parts are calculated.

Using (9) the uncertainty of R_{ac} and L can be given as

$$u^2(R_{\mathrm{ac}}) = \left(\frac{\partial R_{\mathrm{ac}}}{\partial \Re_{\mathrm{reg}}[Z_{21}]}\right)^2 u^2(\Re_{\mathrm{reg}}[Z_{21}]) = u^2(\Re_{\mathrm{reg}}[Z_{21}]) \tag{16}$$

$$u^2(L) = \left(\frac{\partial L}{\partial \Im_{\mathrm{reg}}[Z_{21}]}\right)^2 u^2(\Im_{\mathrm{reg}}[Z_{21}]). \tag{17}$$

The resulting uncertainty of L can be expressed as

$$u^2(L) = \left(\frac{1}{\omega}\right)^2 u^2(\Im_{\mathrm{reg}}[Z_{21}]). \tag{18}$$

Once uncertainty components of the *RL* circuit have been evaluated, the uncertainty of ac–dc difference can be consequently calculated

$$u^2(\delta) = \left(\frac{\partial \delta}{\partial |Z_{\mathrm{shunt}}|}\right)^2 u^2(|Z_{\mathrm{shunt}}|) + \left(\frac{\partial \delta}{\partial R_{\mathrm{dc}}}\right)^2 u^2(R_{\mathrm{dc}}). \tag{19}$$

Then

$$u^2(\delta) = \left(\frac{1}{R_{\mathrm{dc}}}\right)^2 u^2(|Z_{\mathrm{shunt}}|) + \left(\frac{-|Z_{\mathrm{shunt}}|}{R_{\mathrm{dc}}^2}\right)^2 u^2(R_{\mathrm{dc}}) \tag{20}$$

where $u(R_{\mathrm{dc}})$ is the uncertainty component of the dc resistance measurement performed with a digital multimeter. In this paper, its standard value is equal to 1×10^{-6} **Ω**.

The uncertainty of the shunt impedance magnitude $|Z_{\text{shunt}}|$ is given as

$$u^2(|Z_{\text{shunt}}|) = \left(\frac{\partial |Z_{\text{shunt}}|}{\partial R_{\text{ac}}}\right)^2 u^2(R_{\text{ac}}) + \left(\frac{\partial |Z_{\text{shunt}}|}{\partial L}\right)^2 u^2(L) \tag{21}$$

$$u^2(|Z_{\text{shunt}}|) = \left(\frac{R_{\text{ac}}}{\sqrt{R_{\text{ac}}^2 + (L\omega)^2}}\right)^2 u^2(R_{\text{ac}}) + \left(\frac{L\,\omega^2}{\sqrt{R_{\text{ac}}^2 + (L\omega)^2}}\right)^2 u^2(L). \tag{22}$$

The same procedure is used to estimate the uncertainty of phase angle error, leading to

$$u^2(\phi) = \left(\frac{\partial \phi}{\partial R_{\text{ac}}}\right)^2 u^2(R_{\text{ac}}) + \left(\frac{\partial \phi}{\partial L}\right)^2 u^2(L). \tag{23}$$

Then

$$u^2(\phi) = \left(\frac{\omega}{R_{\text{ac}}^2 + (L\omega)^2}\right)^2 [L^2 u^2(R_{\text{ac}}) + R_{\text{ac}}^2 u^2(L)]. \tag{24}$$

B. RC circuit

As explained before, if a current shunt exhibits a predominant capacitive behavior in the frequency range of interest, its complex impedance can be described simply by a resistor–capacitor circuit(*RC* circuit), whose the resistor is connected in parallel with the capacitor. The complex impedance of the shunt is calculated using the following expression:

$$Z_{\text{shunt}} = Z_{21} = \frac{R_{\text{ac}} - j R_{\text{ac}}^2 C\omega}{1 + (R_{\text{ac}} C\omega)^2}. \tag{25}$$

After the polynomial regression, the real and imaginary parts of the shunt impedance (25) can be expressed as

$$\begin{cases} \Re_{\text{reg}}[Z_{21}] = \dfrac{R_{\text{ac}}}{1 + (R_{\text{ac}} C\omega)^2} \\ \Im_{\text{reg}}[Z_{21}] = \dfrac{-R_{\text{ac}}^2 C\omega}{1 + (R_{\text{ac}} C\omega)^2}. \end{cases} \tag{26}$$

The two expressions of (26) are combined to eliminate R_{ac} in the expression of the imaginary part in (26). The capacitor value is calculated by

$$C = \frac{-\Im_{\text{reg}}[Z_{21}]}{\omega\,(\Re_{\text{reg}}^2[Z_{21}] + \Im_{\text{reg}}^2[Z_{21}])}. \tag{27}$$

The ac resistance is calculated by solving a quadratic equation obtained from expression of the real part in (26)

$$R_{\text{ac}}^2(\Re_{\text{reg}}[Z_{21}]\, C^2\omega^2) - R_{\text{ac}} + \Re_{\text{reg}}[Z_{21}] = 0. \tag{28}$$

Because the roots of the polynomial equation are both positive, the solution chosen is the one close to the R_{dc} value of shunt.

Now, we can use the same calculation methods presented in the *RL* circuit to obtain the uncertainties of the resistor R_{ac} and the capacitor C. The uncertainty of C is given as

$$u^2(C) = \left(\frac{2\,\Re_{\text{reg}}[Z_{21}]\,\Im_{\text{reg}}[Z_{21}]}{\omega\,(\Re_{\text{reg}}^2[Z_{21}] + \Im_{\text{reg}}^2[Z_{21}])^2}\right)^2 u^2(\Re_{\text{reg}}[Z_{21}]) + \left(\frac{\Im_{\text{reg}}^2[Z_{21}] - \Re_{\text{reg}}^2[Z_{21}]}{\omega\,(\Re_{\text{reg}}^2[Z_{21}] + \Im_{\text{reg}}^2[Z_{21}])^2}\right)^2 u^2(\Im_{\text{reg}}[Z_{21}]). \tag{29}$$

The uncertainty of R_{ac} is calculated using the solution of a polynomial equation (28)

$$u^2(R_{\text{ac}}) = \left(\frac{-1 + K_3 + \frac{4\,\Re_{\text{reg}}^2[Z_{21}]\,C^2\omega^2}{K_3}}{2\,\Re_{\text{reg}}^2[Z_{21}]\,C^2\omega^2}\right)^2 u^2(\Re_{\text{reg}}[Z_{21}]) + \left(\frac{-1 + K_3 + \frac{2\,\Re_{\text{reg}}^2[Z_{21}]\,C^2\omega^2}{K_3}}{\Re_{\text{reg}}[Z_{21}]\,C^3\omega^2}\right)^2 u^2(C) \tag{30}$$

where

$$K_3 = \sqrt{1 - (2\,\Re_{\text{reg}}[Z_{21}]\,C\omega)^2}. \tag{31}$$

The uncertainty of the ac–dc difference is calculated using (20) where the impedance magnitude uncertainty $u(|Z_{\text{shunt}}|)$ is given as

$$u^2(|Z_{\text{shunt}}|) = \left(\frac{\partial |Z_{\text{shunt}}|}{\partial R_{\text{ac}}}\right)^2 u^2(R_{\text{ac}}) + \left(\frac{\partial |Z_{\text{shunt}}|}{\partial C}\right)^2 u^2(C). \tag{32}$$

The uncertainty $u(|Z_{\text{shunt}}|)$ is therefore expressed as

$$u^2(|Z_{\text{shunt}}|) = \frac{1}{(1 + (R_{\text{ac}}\,C\omega)^2)^3} u^2(R_{\text{ac}}) + \frac{\left(K_4(1 + (R_{\text{ac}}\,C\omega)^2) - R_{\text{ac}}^3\,C\,\omega^2\right)^2}{(1 + (R_{\text{ac}}\,C\omega)^2)^3} u^2(C) \tag{33}$$

where

$$K_4 = \frac{\partial R_{\text{ac}}}{\partial C} = \frac{-1 + K_3 + \frac{2\,\Re_{\text{reg}}^2[Z_{21}]\,C^2\omega^2}{K_3}}{\Re_{\text{reg}}[Z_{21}]\,C^3\omega^2}. \tag{34}$$

The uncertainty of the phase angle error is expressed according to

$$u^2(\phi) = \left(\frac{\partial \phi}{\partial R_{\text{ac}}}\right)^2 u^2(R_{\text{ac}}) + \left(\frac{\partial \phi}{\partial C}\right)^2 u^2(C). \tag{35}$$

Finally, we can calculate the uncertainty of the phase angle by

$$u^2(\phi) = \left(\frac{\omega}{1 + (R_{\text{ac}}\,C\omega)^2}\right)^2 \times [C^2 u^2(R_{\text{ac}}) + (K_4 C + R_{\text{ac}})^2 u^2(C)]. \tag{36}$$

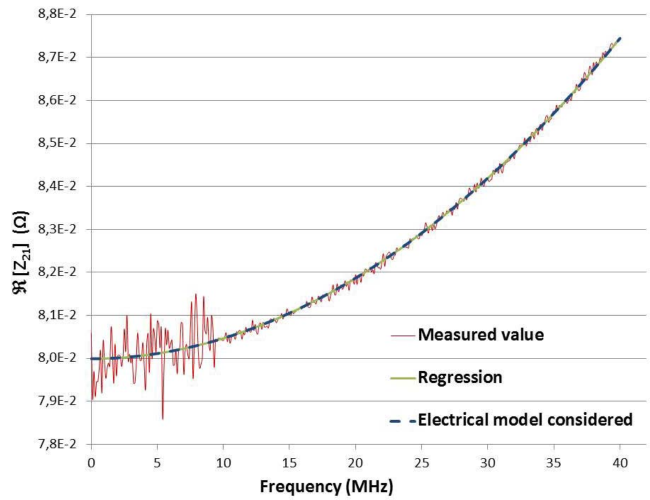

Fig. 4. Real part of the shunt based on a “cage” geometry of 10 A.

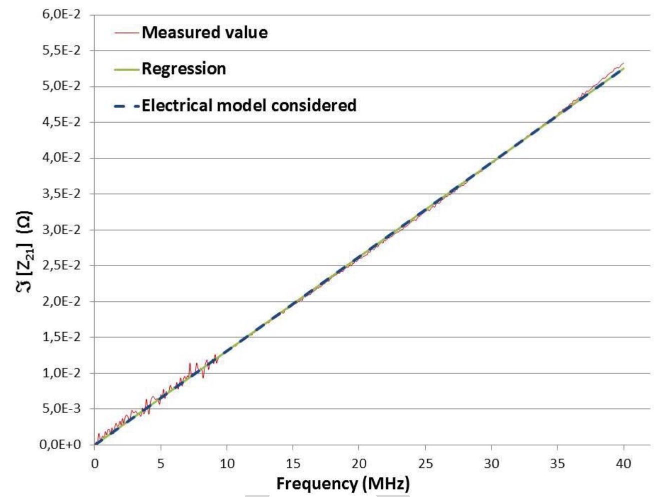

Fig. 5. Imaginary part of the shunt based on a “cage” geometry of 10 A.

V. Experimental Results

AC coaxial shunts based on the “cage” geometry (resistors in parallel within a cage structure) of 10 A and current shunts based on metal electrode leadless face (MELF) resistors from 0.5 up to 10 A have been measured. For clarity of this paper, only the results for a shunt of 10 A obtained are presented and compared to the existing methods in order to validate the approach proposed. It is important to note that comparable results are obtained for other current shunt values.

A VNA E5071C has been calibrated with a calibration kit developed at LNE. The measurements of “cage” and “MELF” current shunts have been performed up to 40 and 60 MHz, respectively. The VNA measurement parameters are:

1) sufficient frequency points (801 points) with a linear distribution;
2) averaging of five measurements at each frequency;
3) intermediate frequency of the VNA receiver equal to 100 Hz.

The method described in this paper has been applied to obtain ac–dc difference and phase angle values and the associated uncertainties. To summarize the experimental approach

1) First, the shunt impedance Z_{21} is calculated from the S-parameters measured with a VNA.
2) Then, the regressed value of the impedance Z_{21} is determined using the values of the electrical model (*RL* or *RC* circuit) which are calculated through the regression approach.
3) Finally, the ac–dc difference and phase angle parameters and its associated uncertainties are calculated.

Figs. 4–7 show the real and imaginary parts measured by the shunt impedance, the regression curves, and the curves obtained from the electrical model considered (*RC* or *RL*). Examples illustrated in Figs. 4–7 concern the 10-A ac coaxial shunts based on “cage” geometry and “MELF” resistors. We can observe measurement noise due to the low value of the 10-A shunt under study which is far from the 50-Ω reference impedance of the VNA and due to the very varied range of S-parameters measured from 9 kHz to 60 MHz: typically, from a few 10^{-4}–10^{-3}. In addition, the noise level becomes abruptly higher below 10 MHz because of the VNA’s internal electronic architecture. (Couplers are different below

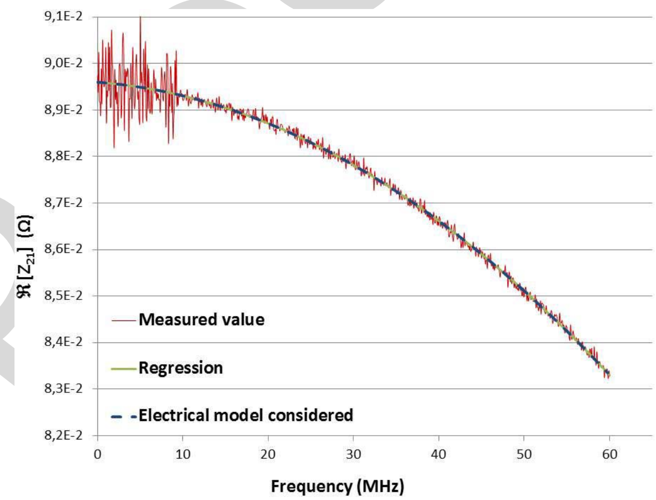

Fig. 6. Real part of the shunt based on “MELF” resistors of 10 A.

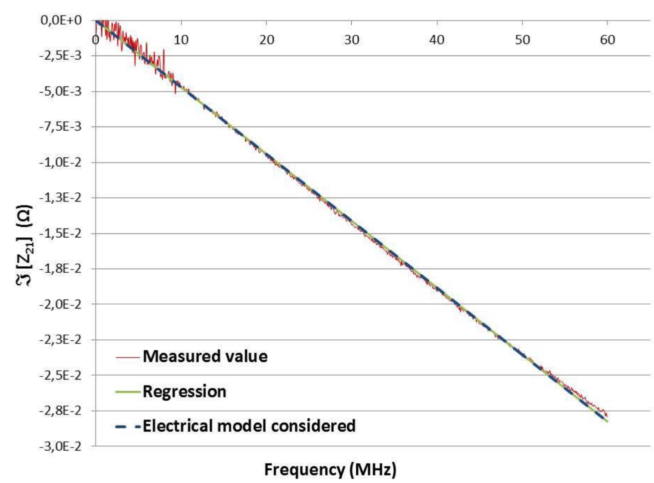

Fig. 7. Imaginary part of the shunt based on “MELF” resistors of 10 A.

TABLE I

CIRCUIT PARAMETERS OF THE MEASURED CURRENT SHUNTS

	DC Resistor value R_{DC} (mΩ)	Inductor value L (pH)	Capacitor value C (nF)
“cage” geometry of 10 A	79.99	209.05 ± 10.17	-
“MELF” resistors of 10 A	89.60	-	9.48 ± 1.11

TABLE II

AC–DC DIFFERENCE RESULTS OF THE AC COAXIAL SHUNT BASED ON A “CAGE” GEOMETRY OF 10 A WITH ITS EXPANDED UNCERTAINTIES AT 100 kHz

	VNA measurement	RISE laboratory measurement	Thermal transfer measurement by LNE
δ (μΩ/Ω)	3.8	62.0	45.5
u(δ) (μΩ/Ω)	199.3	135.0	86.0

TABLE III

PHASE ANGLE RESULTS OF THE AC COAXIAL SHUNT BASED ON A “CAGE” GEOMETRY OF 10 A WITH ITS EXPANDED UNCERTAINTIES AT 100 kHz

	VNA measurement	NMIA laboratory measurement
ϕ (μrad)	1642.0*	1000*
u(ϕ) (μrad)	146.2	124.0

* Values reported in this table concern shunts based on “cage” geometry but manufacturers are different. The shunts measured by NMIA laboratory and using the VNA method are not fabricated on the same design. Phase angle results should be considered as indicative values.

TABLE IV

AC–DC DIFFERENCE RESULTS OF THE CURRENT SHUNT BASED ON MELF RESISTORS OF 10 A WITH ITS EXPANDED UNCERTAINTIES AT 100 kHz

	VNA measurement	JV laboratory measurement	PTB laboratory measurement
δ (μΩ/Ω)	-15.7	-2.0	-18.0
u(δ) (μΩ/Ω)	160.43	11.0	70.0

TABLE V

PHASE ANGLE RESULTS OF THE CURRENT SHUNT BASED ON MELF RESISTORS OF 10 A WITH ITS EXPANDED UNCERTAINTIES AT 100 KHZ

	VNA measurement
ϕ (μrad)	-525.4
u(ϕ) (μrad)	105.0

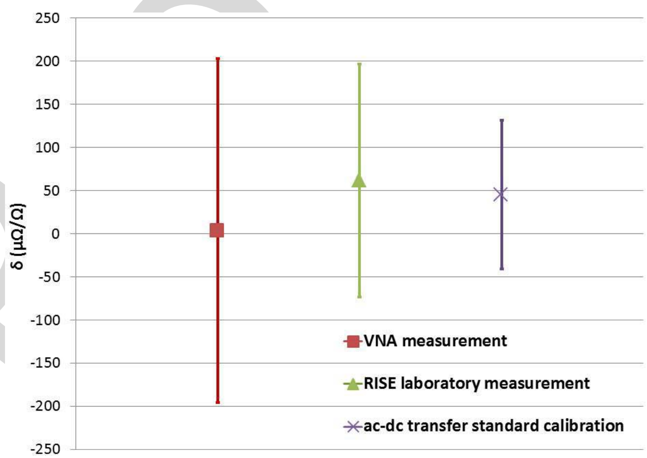

Fig. 8. AC–DC difference results of the current shunt based on a “cage” geometry of 10 A with its expanded at 100 kHz.

and above 10 MHz.) The polynomial regression applied in the presented method allows overcoming the measurement issue related to the noise observed. The curves of the imaginary parts measured are linear and, respectively, negative for shunts based on the “MELF” geometry and positive for shunts based on the “cage” resistor which corresponds to a capacitive and inductive behavior as expected. The real parts are quadratic for both the shunts that can be explained by losses in metallic parts and by the first resonance frequency which is below 300 MHz for both the shunts. Because the frequency resonance is close to the frequency bandwidth used for the polynomial regression, it is noted that the skin effect cannot be quantified from the VNA measurements since there is a combination of resonance and skin effect.

The values of R_{dc}, L, and C calculated are summarized in Table I. The results of ac–dc difference and phase angle parameters and the associated expanded uncertainties ($k = 2$) are presented in Tables II–V. At 100 kHz, the values are higher than those provided by the existing methods. Nevertheless, to our knowledge, the method presented in this paper is the only one able to perform in one step a broadband and simultaneous measurement of the magnitude and phase of current shunts up to a few megahertz with acceptable uncertainties. The measurement method used by the JV and PTB laboratories is a thermal transfer method [24], whereas the RISE laboratory uses a direct comparison method and the NMIA laboratory uses a potentiometer method [9]. The comparison of the ac–dc difference results is shown in Figs. 8 and 9. The results obtained with the VNA method is in very good agreement with the existing methods, particularly for the ac difference results of the current shunt based on “MELF” resistors: the difference of the mean values is significantly less than the uncertainty of the VNA method.

For the existing methods, the shunt parameters are obtained from the electrical current measurement values provided by a reference device. These methods are not able to provide simultaneously both parameters: ac–dc difference and phase angle. Moreover, these methods are mainly limited by the generation of a nominal current at high frequencies. Therefore, uncertainties on ac–dc difference and phase angle parameters depend on the uncertainties related to the high current levels to be produced for the measurements. This constraint explains the limitation of these methods to the low-frequency range (below 100 kHz).

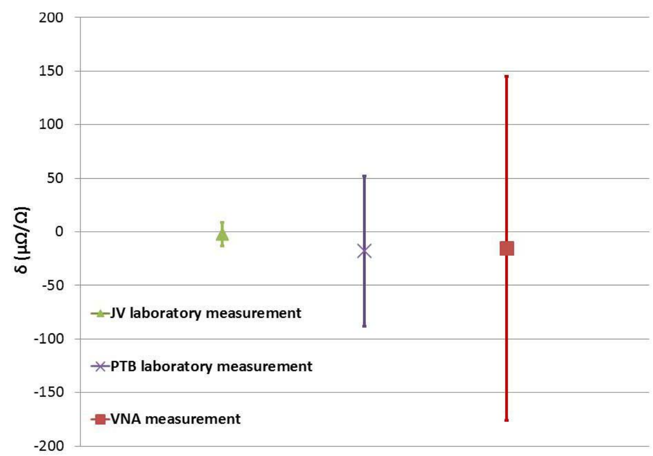

Fig. 9. AC–DC difference results of the current shunt based on MELF resistors of 10 A with its expanded uncertainty at 100 kHz.

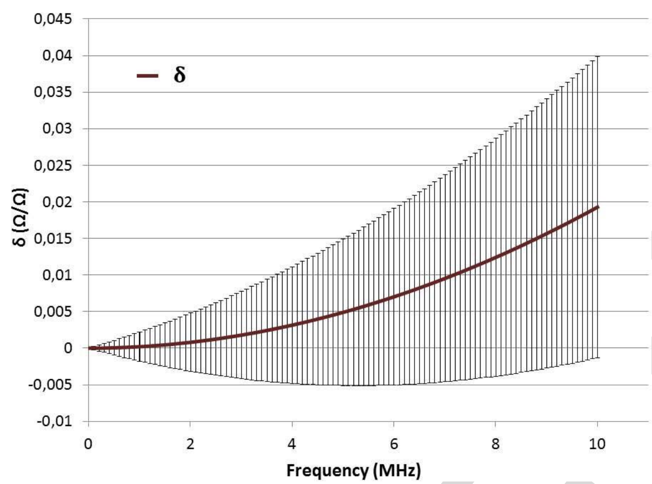

Fig. 10. AC–DC difference with its uncertainties of the ac coaxial shunt based on a "cage" geometry of 10 A up to 10 MHz.

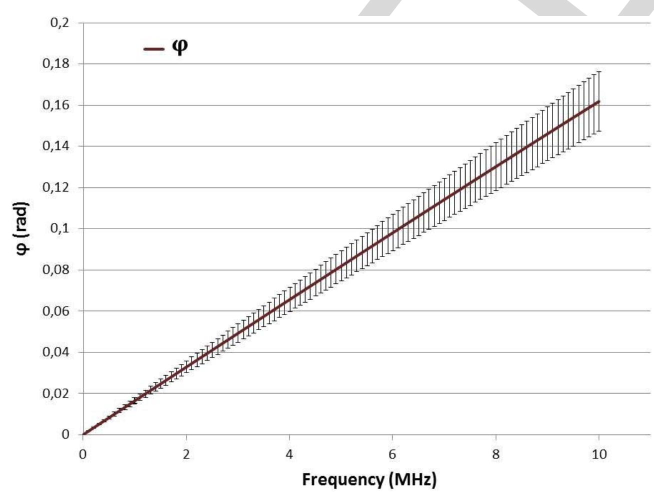

Fig. 11. Phase angle with its uncertainties of the ac coaxial shunt based on a "cage" geometry of 10 A up to 10 MHz.

The proposed method extends the limiting frequency up to a few megahertz. Type A (reproducibility and repeatability intermediate precision conditions of measurement) and type B

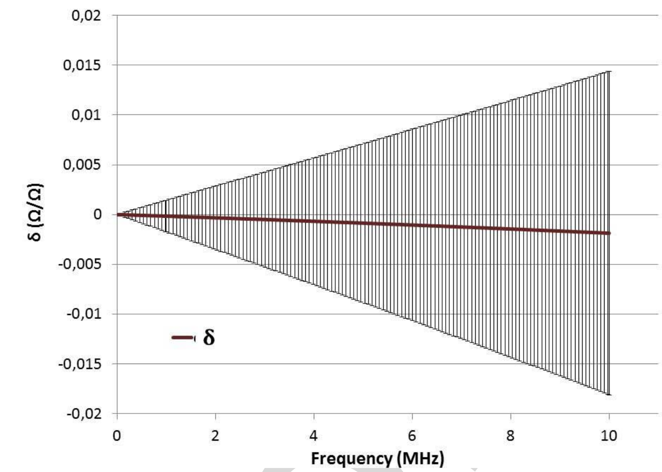

Fig. 12. AC–DC difference with its uncertainties of the current shunt based on MELF resistors of 10 A up to 10 MHz.

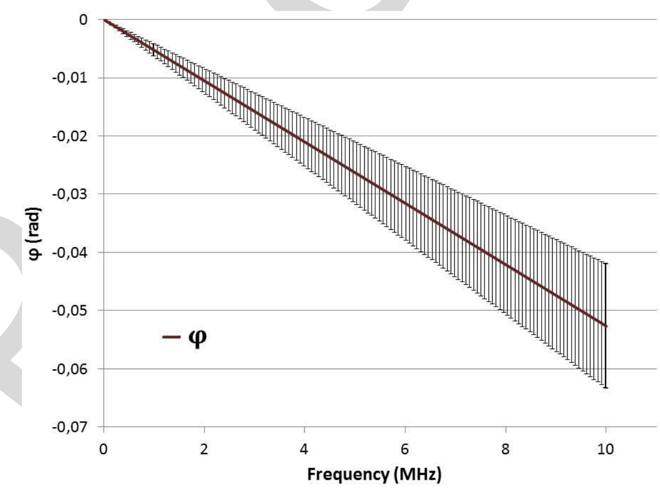

Fig. 13. Phase angle with its uncertainties of the current shunt based on "MELF" resistors of 10 A up to 10 MHz.

uncertainty contributions have been carefully taken into account in the S-parameters uncertainty evaluation. It is important to note that uncertainties of ac–dc difference and phase angle parameters are related to the impedance value of shunt. They are proportional to the inverse of the shunt resistance value [see (20), (22), (33)]. The method described in this paper allows determining simultaneously both the relevant parameters: ac–dc difference and phase angle. The current shunts frequency variation and the associated uncertainties are shown in Figs. 10–13. It can be observed that the frequency resonance impacts more strongly the ac–dc difference results in the case of the shunt based on the "cage" geometry.

VI. CONCLUSION

This paper has presented a new method for measuring and characterizing the standard current shunt up to a few megahertz. This method is based on the use of a VNA. The results of measurements presented in this paper illustrate the effectiveness of this method. Compared with the existing measurement methods, the one proposed has the advantage of increasing the measurement frequency beyond 100 kHz.

Furthermore, it allows to simultaneously measure the ac–dc difference and the phase angle error, which was until now impossible for current levels above 1 A. This method can be applied for current shunts for which a simple equivalent electrical model can be established with a temperature-independent frequency variation and a negligible skin effect on the shunt reactive part in the frequency range of interest. The obtained uncertainty levels are higher to those provided by the existing methods at 100 kHz, but to our knowledge, this new approach is the only one capable of measuring high current shunts in the megahertz frequency range. The Monte Carlo method has been implemented and results compared to the classical GUM approach to validate that the nonlinearity of measurement functions do not impact uncertainties evaluated by the classical GUM method. It is noted that the impact of the nonlinearity on the combined uncertainties depends on the standard deviations of input variables. For instance, if standard deviations are low enough, the nonlinearity can be negligible and the higher orders of the Taylor expansion have not to be considered. If the input variables (S-parameters) of the presented method have too higher standard deviations, the nonlinearity effect should be considered to calculate uncertainties following the classical GUM method or the Monte Carlo method should be applied in this case.

References

[1] K.-E. Rydler, T. Bergsten, and V. Tarasso, "Determination of phase angle errors of current shunts for wideband power measurement," in *Proc. Conf. Precis. Electromagn. Meas.*, Jul. 2012, pp. 284–285.

[2] *The BIPM Key Comparison Database*. accessed: Apr. 2018. [Online]. Available: http://kcdb.bipm.org/

[3] J. R. Kinard, T. E. Lipe, and C. B. Childers, "AC-DC difference relationships for current shunt and thermal converter combinations," in *Proc. Conf. Precis. Electromagn. Meas.*, Jun. 1990, pp. 136–137.

[4] S. Svensson, K.-E. Rydler, and V. Tarasso, "Improved model and phase-angle verification of current shunts for AC and power measurements," in *Proc. Conf. Precis. Electromagn. Meas.*, Jun./Jul. 2004, pp. 82–83.

[5] U. Pogliano, B. Trinchera, and D. Serazio, "Wideband digital phase comparator for high current shunts," *Metrologia*, vol. 49, no. 3, p. 349, 2012.

[6] G. C. Bosco *et al.*, "Phase comparison of high-current shunts up to 100 kHz," *IEEE Trans. Instrum. Meas.*, vol. 60, no. 7, pp. 2359–2365, Jul. 2011.

[7] X. Pan *et al.*, "Measurement of the phase angle errors of high current shunts at frequencies up to 100 kHz," *IEEE Trans. Instrum. Meas.*, vol. 62, no. 6, pp. 1652–1657, Jun. 2013.

[8] B. Pinter, M. Lindič, B. Voljč, Z. Svetik, and R. Lapuh, "Modeling of AC/DC current shunts," in *Proc. CPEM*, Jun. 2010, pp. 599–600.

[9] I. Budovsky, "Measurement of phase angle errors of precision current shunts in the frequency range from 40 Hz to 200 kHz," *IEEE Trans. Instrum. Meas.*, vol. 56, no. 2, pp. 284–288, Apr. 2007.

[10] K.-E. Rydler and V. Tarasso, "A method to determine the phase angle errors of an impedance meter," in *Proc. Conf. Precis. Electromagn. Meas.*, Jun./Jul. 2004, pp. 123–124.

[11] K.-E. Rydler, "High precision automated measuring system for AC-DC current transfer standards," *IEEE Trans. Instrum. Meas.*, vol. 42, no. 2, pp. 608–611, Apr. 1993.

[12] A. Mortara and F. Pythoud, "Wideband accurate calibration of a current probe," in *Proc. Conf. Precis. Electromagn. Meas.*, Jul. 2012, pp. 484–485.

[13] K. Lind, T. Sørsdal, and H. Slinde, "Design, modeling, and verification of high-performance AC–DC current shunts from inexpensive components," *IEEE Trans. Instrum. Meas.*, vol. 57, no. 1, pp. 176–181, Jan. 2008.

[14] L. Scarioni, M. Klonz, and T. Funck, "Quartz planar multijunction thermal converter as a new AC-DC current transfer standard up to 1 MHz," in *Proc. Conf. Precis. Electromagn. Meas.*, Jun./Jul. 2004, pp. 455–456.

[15] D. Fortuné, D. Istrate, F. Ziadé, and I. Blanc, "Measurement method of AC current up to 1 MHz," Tech. Rep., Jan. 2014, pp. 35–39.

[16] F. Ziade, A. Poletaeff, and D. Allal, "Primary standard for S-parameter measurements at intermediate frequencies (IFs)," *IEEE Trans. Instrum. Meas.*, vol. 62, no. 3, pp. 659–666, Mar. 2013.

[17] I. Budovsky, A. M. Gibbes, and D. C. Arthur, "A high-frequency thermal power comparator," *IEEE Trans. Instrum. Meas.*, vol. 48, no. 2, pp. 427–430, Apr. 1999.

[18] *Agilent Network Analyzer Basics*. accessed: Dec. 2017. [Online]. Available: http://www.agilent.com/home

[19] A. Ferrero and U. Pisani, "Two-port network analyzer calibration using an unknown 'thru,'" *IEEE Microw. Guided Wave Lett.*, vol. 2, no. 12, pp. 505–507, Dec. 1992.

[20] D. M. Pozar, *Microwave Engineering*, 4th ed. Hoboken, NJ, USA: Wiley, 2011.

[21] *Evaluation of Measurement Data—Guide to the Expression of Uncertainty in Measurement*, document JCGM 100:2008, BIPM, 2008.

[22] *Evaluation of Measurement Data—Supplement 1 to the 'Guide to the Expression of Uncertainty in Measurement'—Propagation of Distributions Using a Monte Carlo Method*, document JCGM 101, BIPM, 2008.

[23] *The BIPM Key Comparison Database, Calibration and Measurement Capabilities Electricity and Magnetism*, Jan. 2015.

[24] H. Malmbekk, "Final report: EURAMET.EM-S39," *Metrologia*, vol. 52, no. 1A, p. 01003, 2015.

Mohamed Ouameur was born in Ouarzazate, Morocco, in 1990. He received the M.Sc. degree in electrical engineering from Polytech Clermont-Ferrand, Aubière, France, in 2014. He is currently pursuing the Ph.D. degree with the Laboratoire National de Métrologie et d'Essais, Trappes, France.

He was with the Geeps, Laboratoire de Génie Electrique de Paris, Centrale Supélec, CNRS, Université Paris-Sud, Université Paris-Saclay, Gif-sur-Yvettes, France. His current research interests include the traceability of electrical current measurement up to 1 MHz and 10 A.

François Ziade was born in Tremblay-en-France, France, in 1979. He received the M.Sc. degree in applied physics, electronics, and microwave engineering from the University of Pierre et Marie Curie, Paris, France, in 2003, and the Ph.D. degree in electronics and telecommunications from Telecom ParisTech, Paris, in 2008, with a focus on power standards.

In 2007, he joined the Laboratoire National de Métrologie et d'Essais, Trappes, France, as a Researcher. His current research interests include establishing impedance traceability at lower RF, EMC measurements, S-parameters, and terahertz measurements.

Yann Le Bihan received the Ph.D. degree from ENS de Cachan, Cachan, France, in 2000, and the Enabling Degree to supervise Ph.D. Studies (HDR) of Université Paris-Sud, Orsay, France, in 2007.

He was a Former Student with the Aggregation of Electrical Engineering, ENS de Cachan, in 1996. In 2000, he joined the Laboratoire de Génie Electrique de Paris. From 2001 to 2011, he was an Assistant Professor at the IUT de Cachan, Université Paris-Sud, where he has been a Professor since 2011. His current research interests include characterization and nondestructive testing by electromagnetic methods: modeling, sensor design, and inverse problems.

Novel Broadband Calibration Method of Current Shunts Based on VNA

Mohamed Ouameur, François Ziade, and Yann Le Bihan

***Abstract*— Usually high wideband ac current and harmonics measurements are accurately achieved in industry and laboratories by using high accuracy shunts or standard shunts. For particular applications, such as power and transient measurements, it is mandatory to evaluate the shunt impedance phase and magnitude according to the frequency bandwidth of interest before to measure the current with such sensors. High electrical current shunt beyond 1 A is calibrated in magnitude up to 100 kHz and in phase angle up to 200 kHz only by a few National Metrology Institutes. The existing traceable measurement methods to characterize these sensors are limited in frequency to 100 kHz, with expanded uncertainties of the ac–dc difference (magnitude) and the phase angle of more than 5×10^{-6} and 62 μrad at 100 kHz, respectively. A new traceable calibration method to measure and characterize current shunts at high frequencies is presented in this paper. This measurement method is based on the use of a vector network analyzer. The measurements are presented up to 60 MHz, but theoretically, the presented method does not exhibit a specific frequency limitation. Only the characteristics of the shunt under study can impose limitation in practice. While uncertainties are higher than those provided by the existing methods, the method presented in this paper is the only method able to perform in one step a broadband and simultaneous measurement of the magnitude and phase of current shunts up to few megahertz with acceptable uncertainties.**

***Index Terms*— AC–DC difference, calibration method, current measurement, current shunt, phase angle, uncertainty, vector network analyzer (VNA), wideband measurements.**

I. Introduction

INCREASINGLY, it is necessary to measure high levels of currents on a wide frequency bandwidth because of high-current events such as short-circuit transient and impulse currents occurring in many applications such as the development of electric vehicles, and the production, transport, and distribution of energy. This calls for the characterization of wideband current sensors up to the megahertz frequency range. Unfortunately, for high levels of currents, the traceability and the calibration methods of such devices are not available in these extreme frequencies. Up to 1 MHz, the existing methods are designed to measure low current levels (up to 1 A) [1]. For high current levels (beyond 1 A), the measurement frequency bandwidth is limited to 100 kHz [2].

The frequency variation of the impedance Z_{shunt} of a shunt is characterized by [3] as follows.

1) The variation in frequency of the impedance magnitude compared to its dc value (ac–dc difference δ), generally given as
$$\delta = \frac{|Z_{\text{shunt}}| - R_{\text{dc}}}{R_{\text{dc}}} \tag{1}$$
where R_{dc} is the direct current (dc) resistance of the current shunt.
2) The impedance phase angle of the current shunt, defined as [4]
$$\phi = \arctan\left(\frac{\Im[Z_{\text{shunt}}]}{\Re[Z_{\text{shunt}}]}\right) \tag{2}$$
where $\Im$ $[Z_{\text{shunt}}]$ is the imaginary part of the shunt impedance and $\Re$ $[Z_{\text{shunt}}]$ is the real part of the shunt impedance.

Following [3], it is noted that the definition of ac–dc difference δ given in (1) is equivalent to the one recommended by the consultative committee for electricity and magnetism of the International Committee for Weights and Measures (CIPM). The definition given in (1) has been used since the method presented in this paper is based on the impedance modeling of current shunts which are calibrated.

II. Existing Calibration Methods of Shunts

Metrologically, the existing calibration methods deliver very good results up to typically 100 kHz and 1 A [5]–[8] but only one parameter is measured: either the ac–dc difference or the phase angle. We can briefly classify the existing shunt measurement methods in the following categories.

A. Direct Comparison Method

The principle of this method is based on the direct comparison of voltages measured between terminals of two series connected shunts: one ac shunt standard and one ac shunt under test being calibrated. The range of voltages is identical for both devices during the calibration process.

This method has been used to measure the absolute phase angle errors between 100 and 300 mA up to 1 MHz of current shunts based on a "cage" topology of resistors [1]. To assess the phase angle error, a phase comparator has been

Manuscript received December 19, 2017; revised April 10, 2018; accepted June 19, 2018. The Associate Editor coordinating the review process was Dr. Thomas Lipe. *(Corresponding author: François Ziade.)*

M. Ouameur is with the Laboratoire National deMétrologie et d'Essais, 78197 Trappes, France, and also with GeePs, Laboratoire Génie Electrique et Electronique de Paris, 91192 Gif-sur-Yvette, France (e-mail: francois.ziade@lne.fr).

F. Ziade is with the Laboratoire National deMétrologie et d'Essais, 78197 Trappes, France.

Y. L. Bihan is with GeePs, Laboratoire Génie Electrique et Electronique de Paris, 91192 Gif-sur-Yvette, France (e-mail: yann.le-bihan@geeps.centralesupelec.fr).

Color versions of one or more of the figures in this paper are available online at http://ieeexplore.ieee.org.

Digital Object Identifier 10.1109/TIM.2018.2855499

developed based on [1], [4], [6], [9], and [10]. The two current shunts to be compared are connected in series using a current T-connector in a measurement setup composed of an ac current source and two 2-channel digitizers. The expanded uncertainty ($k = 2$) of the phase angle error is ± 200 μrad at 1 MHz.

A wideband phase comparator has been developed in order to perform phase angle measurements with higher levels of current [5] from 2 to 100 A and for frequencies from 500 Hz to 100 kHz [6]. The expanded uncertainty ($k = 2$) of the phase angle error is ± 50 μrad at 100 kHz for levels of current up to 10 A.

An automated measuring system has been developed to assess the impedance magnitude deviation from dc of ac–dc current transfer standards. The principle is based on the connection of the two thermal current converters. The difference between the output of the current converters and the back-off voltages are measured by nano-voltmeters [11]. The uncertainty of ac–dc difference is estimated less than ± 50 mA/A for currents up to 30 mA and frequencies up to 100 kHz.

Generally, the direct comparison method suffers from the existence of a reversal error occurring when the relative positions of the two current shunts are reversed [12]. Accordingly, one approach has been developed and applied to compare current outputs from an ac shunt standard with a current probe [12]. The ac–dc difference of "cage" current shunts has been found to be less than 10 ppm up to 100 kHz without giving an estimated uncertainty.

B. Thermal Transfer Method

The thermal transfer method is commonly used in the National Metrology Institutes (NMIs) to measure alternating voltage or ac current up to the megahertz range. The measurement method, based on a thermocouple, measures the continuous value of the electric quantity (current or voltage) which causes the same heating effect generated by the alternating value to be assessed.

In 2011, results of various existing shunts have been published [6] on the basis of the thermal transfer method. The shunts used for the ac–dc current transfer are of planar multijunction thermal converters type (PMJTC) [13], [14]. The PMJTC type is used to obtain the lowest uncertainties of the measurement, but these are not easily available commercially. The expanded uncertainty of the ac–dc difference is preliminarily estimated to be 9 μA/A from 10 Hz to 100 kHz for current levels ranging from 30 mA to 10 A.

A resonant method has been developed to calibrate current probes at a current level of 10 A and frequencies up to 1 MHz [15]. In this method, a 1-Ω resistor is characterized by the thermal transfer method up to 100 kHz and using a VNA traceable to International System of units (SI) in the megahertz range [16]. The reported uncertainties are of 2% at 1 MHz.

C. Potentiometer method

Another measurement method has been developed to characterize the phase angle of current shunts from 40 Hz to 200 kHz [9]. This approach is based on the use of 3-D multijunction thermal converters (TPC), precision amplifiers, and a specialized measurement algorithm [17]. The uncertainties of the phase angle are 141 μrad from 100 mA to 20 A, at frequencies from 40 Hz to 200 kHz.

At current levels of 10 A and 100 kHz, the existing measurement methods previously published by different NMIs for measuring the phase angle, and ac–dc difference exhibits an expanded uncertainty ($k = 2$) of at least 62 μrad and 6 ppm, respectively. Currently, no existing method enables to measure simultaneously the ac–dc difference and the phase angle. These approaches are limited to 200 kHz for current levels exceeding 10 A. Furthermore, the traceability to the SI for most methods is not completely achieved beyond 100 kHz.

In this paper, we present a new measurement method adapted for characterizing simultaneously the ac–dc difference and phase angle of current shunts up to a few megahertz. In what follows we will present successively the method, the uncertainty calculation, and the measurement results.

III. SHUNT CALIBRATION METHOD USING AVNA

The proposed calibration method is based on a vector network analyzer (VNA) which has some attractive features such as low sweep time, broad frequency bandwidth, and capability of measuring complex S-parameters. The proposed method requires the measurement of S-parameters from the lowest available frequency (below a few tens of kilohertz) up to a few tens of megahertz. Practically, an Agilent E5071C with a frequency bandwidth ranging from 9 kHz to 4.5 GHz is used for the measurements. The S-parameter uncertainty of a VNA is impacted by systematic error terms: directivity, source match, reflection tracking, transmission tracking, and load match [18]. Before using a VNA, a calibration method is mandatory to remove the systematic errors. The unknown thru method [19] is used to calibrate the VNA from 9 kHz to 100 MHz. The unknown thru calibration method is based on the use of three impedance standards (open, short, and 50-Ω loads) and an additional unknown thru connection. This latter is a transmission line for which the characteristics are determined during the calibration process. The traceability of the VNA measurements is established through the precise knowledge of the 50-Ω impedance standard according to the frequency [16] and using a type *N* calibration kit completely calculable from dc to 1 GHz [2]. Once the VNA is calibrated, the shunt is simply connected to the VNA and its S-matrix measured on the frequency bandwidth of interest. The system for measuring the S-parameters of a two-port shunt is shown in Fig. 1.

Generally, the impedance Z_{shunt} of a two-port shunt is defined by its transmission impedance Z_{21} from port 1 (current input) to port 2 (voltage output). Therefore, this impedance is calculated from the S-parameter values measured with a VNA. The impedance of the 50-Ω load standard used during the VNA calibration is completely calculable and traceable to SI. The variation of real and imaginary parts of the load standard impedance is very low. It follows that S-parameters measurements of a shunt can be accurately normalized to the

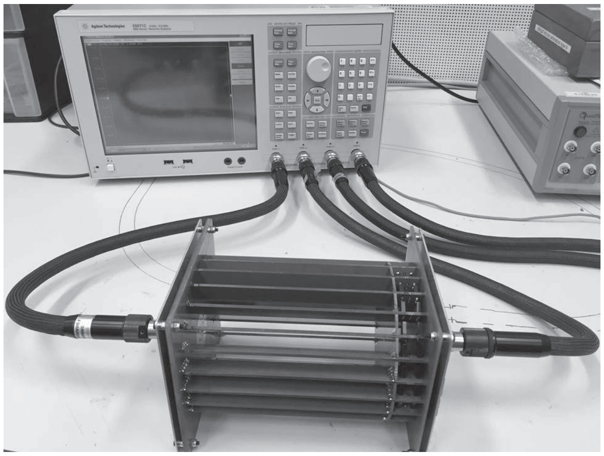

Fig. 1. Measurement of the S-parameters of an ac coaxial shunt based on a "cage" geometry using a VNA.

characteristic impedance Z_0 equal to 50 Ω. After calibration of the VNA, the reference planes of S-parameters measurement correspond to current and voltage connectors of the current shunt. Hence, S-parameters that are determined this way are intrinsic characteristics of the shunt: they characterize the shunt itself independently of the VNA input impedance. Finally, values of the transfer impedance Z_{21}, and consequently, values of the shunt's model determined using the S-parameters are independent of the VNA input impedance. Using the method presented in this paper, shunts are characterized as four-terminal impedance and it is not required to consider any loading errors. The transfer impedance Z_{21} (Z_{shunt}) is expressed from S-parameters and the characteristic impedance Z_0 is equal to 50 Ω [20]

$$Z_{21} = Z_0 \frac{2\, S_{21}}{(1 - S_{11})(1 - S_{22}) - S_{12} S_{21}}. \tag{3}$$

The real and imaginary parts of S-parameters of the current shunt are measured and stored for data postprocessing. For the calculations, the following notations are used:

$$\begin{cases} S_{11} = \alpha_{11} + j\beta_{11} \\ S_{12} = \alpha_{12} + j\beta_{12} \\ S_{21} = \alpha_{21} + j\beta_{21} \\ S_{22} = \alpha_{22} + j\beta_{22} \end{cases} \tag{4}$$

The real and imaginary parts of the measured shunt impedance Z_{21} can be expressed by

$$\begin{cases} \Re_{\text{mes}}[Z_{21}] = 2\ Z_0 \dfrac{\alpha_{21} K_1 + \beta_{21} K_2}{K_1^2 + K_2^2} \\ \Im_{\text{mes}}[Z_{21}] = 2\ Z_0 \dfrac{\beta_{21} K_1 - \alpha_{21} K_2}{K_1^2 + K_2^2} \end{cases} \tag{5}$$

where

$$K_1 = 1 - \alpha_{11} - \alpha_{22} + \alpha_{11}\alpha_{22} - \beta_{11}\beta_{22} - \alpha_{12}\alpha_{21} + \beta_{12}\beta_{21} \tag{6}$$

$$K_2 = \alpha_{11}\beta_{22} + \alpha_{22}\beta_{11} - \beta_{11} - \beta_{22} - \alpha_{12}\beta_{21} - \alpha_{21}\beta_{12}. \tag{7}$$

The VNA has a standard output impedance of 50 Ω, whereas the impedance of the current shunt is generally observed to

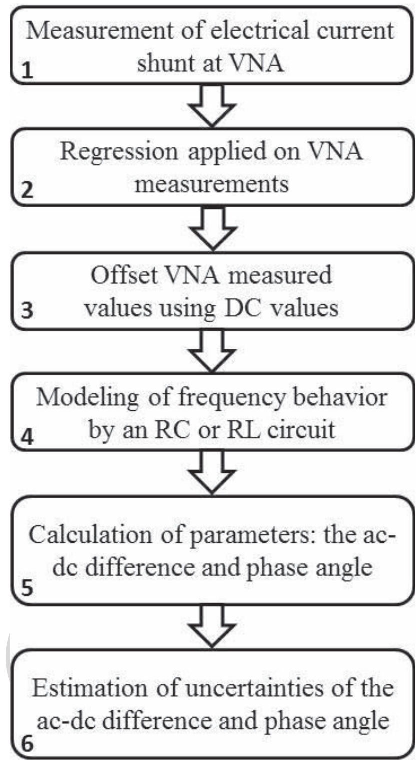

Fig. 2. Steps of the proposed measurement method.

be less than 2 Ω. For instance, the device under test (DUT) presented in Fig. 1 is an ac coaxial current shunt of 10 A based on the cage geometry with a dc resistance nominal value of 0.08 Ω [4]. This impedance deviation between the DUT and VNA produces noise and low accuracy in measurements. As it stands, VNA measurement data cannot be used directly to assess shunt parameters.

The purpose of this new measurement method is to prevent the effect of the mismatch between the shunt and the VNA output impedance by applying a regression on VNA measurements data and providing modeling of the shunt. The description of the method is detailed as follows (Fig. 2).

Step 1: The shunt to be calibrated is measured with a VNA. An average of 10 measurements is calculated to reduce the connectors' repeatability error.

Step 2: A polynomial regression is applied to the VNA measurements. The influence of the measurement noise is reduced using a regression: linear for the imaginary part and polynomial of degree two for the real part. The polynomial and linear regression have been validated by using Pearson's chi-squared test.

*Step 3:*The regressed curves are shifted to match the dc value of the shunt. The use of the VNA is indeed mainly aimed at evaluating the variation in frequency, because the dc value of the shunt cannot be measured directly and exactly with a VNA and is instead measured with a Digital Multimeter standard calibrated.

Step 4: A model of the measured shunt is obtained by calculating the values of an equivalent circuit of the shunt constituted of either an *RL* circuit (a resistor in series with

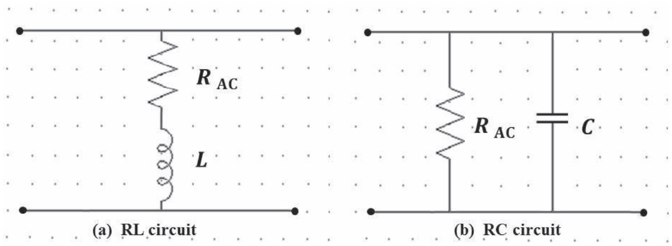

Fig. 3. Equivalent circuit of the shunt considered. (a) *RL* circuit. (b) *RC* circuit.

an inductor) or an *RC* circuit (a resistor in parallel with a capacitor) (Fig. 3). The choice of the equivalent circuit configuration is based on the sign of the imaginary part of the measured shunt impedance: for instance, if the imaginary part of the shunt impedance is negative, a circuit model (R, C) is applied.

Step 5: The determination of the electrical equivalent model allows calculating the values of the ac–dc difference and phase angle with low associated uncertainties.

Step 6: Uncertainty calculation associated with this measurement method is finally calculated. The calculation is detailed in Section IV.

The shunt can be calibrated between dc and a few tens of megahertz depending on its frequency variation. In this paper, the frequency limit for the measurements does not exceed 60 MHz for which the wavelength λ is approximately 5 m. The shunt's length considered in this paper is less than 30 cm. In a general way, the transmission line theory could be applied to calculate Z_{21} but as shown in Section V, a simple (R, L) or (R, C) equivalent circuits of a shunt is appropriate and accurate to model Z_{21} because structures and values of the modeling are directly determined from measurements. Consequently, potential transmission line effects are taken into account in this case.

In the case of (R, L) circuit, the shunt inductance is composed of the two following: internal and external inductances. In a general way, internal inductance is dependent on skin effects, but in the shunts considered in this paper, the external inductance is the most preponderant inductance and is independent of the frequency. The validity of this approximation is observed in the imaginary part measured: the reactance is linear according to the frequency range of interest. The linear regression applied to the reactance part has been validated by the statistical Pearson's chi-squared test (Figs. 5 and 7). In this particular case, the skin effect can be considered as negligible on the reactive part of Z_{shunt}.

In practice, the frequency limitations of the method are linked to current shunt:

1) presenting a simple equivalent electrical model (*RL* or *RC*);
2) having a temperature-independent frequency variation;
3) characterized by a negligible skin effect on the reactive part of Z_{shunt} in the frequency range of interest.

In a general way, the resistance part of a shunt is subject to variation mainly due to resonance and skin effect at high frequencies. Different shunts considered in this paper have a frequency variation that can be approximated using a second-degree polynomial regression. This latter has been validated by performing the statistical Pearson's chi-squared test: the regression describes appropriately the measurements taking into account the standard deviation.

IV. Uncertainty Calculation

The uncertainty evaluation of ac–dc difference and phase angle has been achieved according to the "evaluation of measurement data—a guide to the expression of uncertainty in measurement" (GUM) [21]. The experimental measurement values are considered to calculate the standard deviation of each variable from the equivalent electrical model and finally to evaluate uncertainties on ac–dc difference and phase angle parameters. The presented method involves nonlinear measurement functions for the measurands: ac–dc difference and phase angle. The law of propagation of uncertainty based on a first-order Taylor series expansion can leads to incorrect standard uncertainties of the results when nonlinear measurement functions are involved in the calculation. Indeed, if the nonlinearity of functions is significant, higher order terms in the Taylor series expansion must be included in the expression of the combined standard uncertainty. In this paper, it has been verified that the nonlinearity does not affect significantly the combined uncertainties of the two measurands (ac–dc difference and phase angle) calculated with the first-order Taylor series expansion. This verification has been performed according to the method described in GUM supplement 1 [22]: it consists of applying the Monte Carlo method using one million samples to calculate the distribution of the measurand. Once the distribution is obtained, the mean, the standard deviation, and the 95% confidence interval can be calculated and compared to the classical law of propagation of uncertainty results. The calculation has been performed to the following frequencies 100 kHz, 1 MHz, 10 MHz, and 40 MHz and compared to the GUM classical results. The normal distribution obtained by the Monte Carlo method validates the use of a coverage factor of 2. The difference between the two approaches is negligible and demonstrates that the first-order Taylor series approximation can be applied to calculate the combined standard uncertainty presented in this novel broadband calibration method of current shunts based on VNA. Considering the number of frequency measurement points and the use of a polynomial regression, the Monte Carlo method is time-consuming which justifies the implementation of the classical GUM approach.

Different types A and B uncertainty contributions considered in our calculation are the following.

1) Repeatability condition of measurement (type A):
   a) The VNA has been calibrated one time and ten measurements have been performed in a very short time by connecting and disconnecting connectors between each measurement.
2) The intermediate precision condition of measurement (type A):

a) The VNA has been calibrated one time each day for three consecutive days and measurements have been performed after each calibration.

3) Reproducibility condition of measurement (type A):

a) The VNA has been calibrated and measurements performed by two different operators.

b) Two different measurements have been performed using two different VNAs (change in the measuring systems) and cables.

c) Two different calibration kits have been used to calibrate and perform two different sets of measurements

4) Accuracy of the standards modeling (type B).

5) Correlation of S-parameters (type B).

6) Errors related to the interpolation process (type B).

7) Errors of the shunt modeling (type B).

A. RL Circuit

As explained before, if a current shunt exhibits a predominant inductive behavior in the frequency range of interest, its complex impedance can be described simply by a resistor–inductor series circuit (*RL* circuit)

$$Z_{21} = R_{\mathrm{ac}} + jL\omega \tag{8}$$

where R_{ac} and L are, respectively, the ac resistor and inductor of the considered *RL* circuit. R_{ac} and L are given as

$$\begin{cases} R_{\mathrm{ac}} = \Re_{\mathrm{reg}}[Z_{21}] \\ L = \dfrac{\Im_{\mathrm{reg}}[Z_{21}]}{\omega} \end{cases} \tag{9}$$

where $\Im_{\mathrm{reg}}[Z_{21}]$ and $\Re_{\mathrm{reg}}[Z_{21}]$ result from the linear regression of the imaginary part and from the polynomial regression of degree 2 of the real part of the shunt impedance, respectively. The real and imaginary parts can be expressed in terms of the regression coefficients and the frequency as

$$\begin{cases} \Re_{\mathrm{reg}}[Z_{21}] = a_0 + a_1 f + a_2 f^2 \\ \Im_{\mathrm{reg}}[Z_{21}] = b_1 f \end{cases} \tag{10}$$

where a_i and b_1 are, respectively, the polynomial regression coefficients of the real part and linear regression coefficient of the imaginary part, and f is the frequency.

The polynomial degrees are chosen using the frequency behavior of the shunt to be characterized. Noting that in dc, the real and imaginary parts are equal, respectively, to the measured value by a digital multimeter ($R_{\mathrm{dc}} = a_0$) and to zero.

Finally, the expressions in (10) permit to calculate the regression uncertainties using uncertainty propagation, such as

$$\begin{aligned} &u^2(\mathrm{R}_{\mathrm{reg}}[Z_{21}]) \\ &\quad = \left(\frac{\partial \mathrm{R}_{\mathrm{reg}}[Z_{21}]}{\partial a_0}\right)^2 u^2(a_0) + \left(\frac{\partial \mathrm{R}_{\mathrm{reg}}[Z_{21}]}{\partial a_1}\right)^2 u^2(a_1) \\ &\qquad + \left(\frac{\partial \mathrm{R}_{\mathrm{reg}}[Z_{21}]}{\partial a_2}\right)^2 u^2(a_2) + \left(\frac{\partial \mathrm{R}_{\mathrm{reg}}[Z_{21}]}{\partial f}\right)^2 u^2(f) \end{aligned} \tag{11}$$

where $u(x)$ is the standard uncertainty of the parameter x.

The uncertainty of the frequency parameter is negligible compared to the other components of uncertainty.

Consequently, (11) can be expressed as

$$u^2(\Re_{\mathrm{reg}}[Z_{21}]) = u^2(a_0) + f^2 u^2(a_1) + f^4 u^2(a_2). \tag{12}$$

For the imaginary part, from (10), we can express its uncertainty as

$$u^2(\Im_{\mathrm{reg}}[Z_{21}]) = \left(\frac{\partial \Im_{\mathrm{reg}}[Z_{21}]}{\partial b_1}\right)^2 u^2(b_1) = f^2 u^2(b_1). \tag{13}$$

The uncertainty of the regression coefficients is estimated by a standard error (square root of a variance) [**?**]. These uncertainties depend on the measurement uncertainties of the real $u(R_{\mathrm{mes}})$ and imaginary $u(I_{\mathrm{mes}})$ parts of the measured impedance Z_{21}. $u(R_{\mathrm{mes}})$ and $u(I_{\mathrm{mes}})$ are propagated from the uncertainty of the S-parameters measured with a VNA.

The measurement uncertainties of the real $u(R_{\mathrm{mes}})$ and imaginary u(I_{mes}) parts of Z_{21} are calculated by

$$u^2(\Re_{\mathrm{mes}}[Z_{21}]) = \sum_{i=1}^{2}\sum_{j=1}^{2}\left(\begin{array}{l} \left(\frac{\partial \Re_{\mathrm{mes}}[Z_{21}]}{\partial \alpha_{ij}}\right)^2 u^2(\alpha_{ij}) \\ + \left(\frac{\partial \Re_{\mathrm{mes}}[Z_{21}]}{\partial \beta_{ij}}\right)^2 u^2(\beta_{ij}) \end{array}\right) \tag{14}$$

$$u^2(\Im_{\mathrm{mes}}[Z_{21}]) = \sum_{i=1}^{2}\sum_{j=1}^{2}\left(\begin{array}{l} \left(\frac{\partial \Im_{\mathrm{mes}}[Z_{21}]}{\partial \alpha_{ij}}\right)^2 u^2(\alpha_{ij}) \\ + \left(\frac{\partial \Im_{\mathrm{mes}}[Z_{21}]}{\partial \beta_{ij}}\right)^2 u^2(\beta_{ij}) \end{array}\right) \tag{15}$$

where $u(\alpha_{ij})$ and $u(\beta_{ij})$ are the standard uncertainty of real and imaginary parts of S-parameters measured. These uncertainties are those obtained using a calibration kit developed at LNE to calibrate the VNA: standard uncertainties of u(α ij) and u(β ij) ranges from 5.10-5 to 5.10-2 and 8.10-5 to 0.25 respectively. The covariance matrices between real and imaginary parts are calculated.

Using (9) the uncertainty of R_{ac} and L can be given as

$$u^2(R_{\mathrm{ac}}) = \left(\frac{\partial R_{\mathrm{ac}}}{\partial \Re_{\mathrm{reg}}[Z_{21}]}\right)^2 u^2(\Re_{\mathrm{reg}}[Z_{21}]) = u^2(\Re_{\mathrm{reg}}[Z_{21}]) \tag{16}$$

$$u^2(L) = \left(\frac{\partial L}{\partial \Im_{\mathrm{reg}}[Z_{21}]}\right)^2 u^2(\Im_{\mathrm{reg}}[Z_{21}]). \tag{17}$$

The resulting uncertainty of L can be expressed as

$$u^2(L) = \left(\frac{1}{\omega}\right)^2 u^2(\Im_{\mathrm{reg}}[Z_{21}]). \tag{18}$$

Once uncertainty components of the *RL* circuit have been evaluated, the uncertainty of ac–dc difference can be consequently calculated

$$u^2(\delta) = \left(\frac{\partial \delta}{\partial |Z_{\mathrm{shunt}}|}\right)^2 u^2(|Z_{\mathrm{shunt}}|) + \left(\frac{\partial \delta}{\partial R_{\mathrm{dc}}}\right)^2 u^2(R_{\mathrm{dc}}). \tag{19}$$

Then

$$u^2(\delta) = \left(\frac{1}{R_{\mathrm{dc}}}\right)^2 u^2(|Z_{\mathrm{shunt}}|) + \left(\frac{-|Z_{\mathrm{shunt}}|}{R_{\mathrm{dc}}^2}\right)^2 u^2(R_{\mathrm{dc}}) \tag{20}$$

where $u(R_{\mathrm{dc}})$ is the uncertainty component of the dc resistance measurement performed with a digital multimeter. In this paper, its standard value is equal to $1 \times 10^{-6}\ \Omega$.

The uncertainty of the shunt impedance magnitude $|Z_{\text{shunt}}|$ is given as

$$u^2(|Z_{\text{shunt}}|) = \left(\frac{\partial |Z_{\text{shunt}}|}{\partial R_{\text{ac}}}\right)^2 u^2(R_{\text{ac}}) + \left(\frac{\partial |Z_{\text{shunt}}|}{\partial L}\right)^2 u^2(L) \tag{21}$$

$$u^2(|Z_{\text{shunt}}|) = \left(\frac{R_{\text{ac}}}{\sqrt{R_{\text{ac}}^2 + (L\omega)^2}}\right)^2 u^2(R_{\text{ac}}) + \left(\frac{L\,\omega^2}{\sqrt{R_{\text{ac}}^2 + (L\omega)^2}}\right)^2 u^2(L). \tag{22}$$

The same procedure is used to estimate the uncertainty of phase angle error, leading to

$$u^2(\phi) = \left(\frac{\partial \phi}{\partial R_{\text{ac}}}\right)^2 u^2(R_{\text{ac}}) + \left(\frac{\partial \phi}{\partial L}\right)^2 u^2(L). \tag{23}$$

Then

$$u^2(\phi) = \left(\frac{\omega}{R_{\text{ac}}^2 + (L\omega)^2}\right)^2 [L^2 u^2(R_{\text{ac}}) + R_{\text{ac}}^2 u^2(L)]. \tag{24}$$

B. RC circuit

As explained before, if a current shunt exhibits a predominant capacitive behavior in the frequency range of interest, its complex impedance can be described simply by a resistor–capacitor circuit(*RC* circuit), whose the resistor is connected in parallel with the capacitor. The complex impedance of the shunt is calculated using the following expression:

$$Z_{\text{shunt}} = Z_{21} = \frac{R_{\text{ac}} - j R_{\text{ac}}^2 C\omega}{1 + (R_{\text{ac}} C\omega)^2}. \tag{25}$$

After the polynomial regression, the real and imaginary parts of the shunt impedance (25) can be expressed as

$$\begin{cases} \Re_{\text{reg}}[Z_{21}] = \dfrac{R_{\text{ac}}}{1 + (R_{\text{ac}} C\omega)^2} \\ \Im_{\text{reg}}[Z_{21}] = \dfrac{-R_{\text{ac}}^2 C\omega}{1 + (R_{\text{ac}} C\omega)^2}. \end{cases} \tag{26}$$

The two expressions of (26) are combined to eliminate R_{ac} in the expression of the imaginary part in (26). The capacitor value is calculated by

$$C = \frac{-\Im_{\text{reg}}[Z_{21}]}{\omega\,(\Re_{\text{reg}}^2[Z_{21}] + \Im_{\text{reg}}^2[Z_{21}])}. \tag{27}$$

The ac resistance is calculated by solving a quadratic equation obtained from expression of the real part in (26)

$$R_{\text{ac}}^2(\Re_{\text{reg}}[Z_{21}]\, C^2\omega^2) - R_{\text{ac}} + \Re_{\text{reg}}[Z_{21}] = 0. \tag{28}$$

Because the roots of the polynomial equation are both positive, the solution chosen is the one close to the R_{dc} value of shunt.

Now, we can use the same calculation methods presented in the *RL* circuit to obtain the uncertainties of the resistor R_{ac} and the capacitor C. The uncertainty of C is given as

$$u^2(C) = \left(\frac{2\,\Re_{\text{reg}}[Z_{21}]\,\Im_{\text{reg}}[Z_{21}]}{\omega\,(\Re_{\text{reg}}^2[Z_{21}] + \Im_{\text{reg}}^2[Z_{21}])^2}\right)^2 u^2(\Re_{\text{reg}}[Z_{21}]) + \left(\frac{\Im_{\text{reg}}^2[Z_{21}] - \Re_{\text{reg}}^2[Z_{21}]}{\omega\,(\Re_{\text{reg}}^2[Z_{21}] + \Im_{\text{reg}}^2[Z_{21}])^2}\right)^2 u^2(\Im_{\text{reg}}[Z_{21}]). \tag{29}$$

The uncertainty of R_{ac} is calculated using the solution of a polynomial equation (28)

$$u^2(R_{\text{ac}}) = \left(\frac{-1 + K_3 + \frac{4\,\Re_{\text{reg}}^2[Z_{21}]\,C^2\omega^2}{K_3}}{2\,\Re_{\text{reg}}^2[Z_{21}]\,C^2\omega^2}\right)^2 u^2(\Re_{\text{reg}}[Z_{21}]) + \left(\frac{-1 + K_3 + \frac{2\,\Re_{\text{reg}}^2[Z_{21}]\,C^2\omega^2}{K_3}}{\Re_{\text{reg}}[Z_{21}]\,C^3\omega^2}\right)^2 u^2(C) \tag{30}$$

where

$$K_3 = \sqrt{1 - (2\,\Re_{\text{reg}}[Z_{21}]\,C\omega)^2}. \tag{31}$$

The uncertainty of the ac–dc difference is calculated using (20) where the impedance magnitude uncertainty $u(|Z_{\text{shunt}}|)$ is given as

$$u^2(|Z_{\text{shunt}}|) = \left(\frac{\partial |Z_{\text{shunt}}|}{\partial R_{\text{ac}}}\right)^2 u^2(R_{\text{ac}}) + \left(\frac{\partial |Z_{\text{shunt}}|}{\partial C}\right)^2 u^2(C). \tag{32}$$

The uncertainty $u(|Z_{\text{shunt}}|)$ is therefore expressed as

$$u^2(|Z_{\text{shunt}}|) = \frac{1}{(1 + (R_{\text{ac}}\,C\omega)^2)^3} u^2(R_{\text{ac}}) + \frac{\left(K_4(1 + (R_{\text{ac}}\,C\omega)^2) - R_{\text{ac}}^3\,C\,\omega^2\right)^2}{(1 + (R_{\text{ac}}\,C\omega)^2)^3} u^2(C) \tag{33}$$

where

$$K_4 = \frac{\partial R_{\text{ac}}}{\partial C} = \frac{-1 + K_3 + \frac{2\,\Re_{\text{reg}}^2[Z_{21}]\,C^2\omega^2}{K_3}}{\Re_{\text{reg}}[Z_{21}]\,C^3\omega^2}. \tag{34}$$

The uncertainty of the phase angle error is expressed according to

$$u^2(\phi) = \left(\frac{\partial \phi}{\partial R_{\text{ac}}}\right)^2 u^2(R_{\text{ac}}) + \left(\frac{\partial \phi}{\partial C}\right)^2 u^2(C). \tag{35}$$

Finally, we can calculate the uncertainty of the phase angle by

$$u^2(\phi) = \left(\frac{\omega}{1 + (R_{\text{ac}}\,C\omega)^2}\right)^2 \times [C^2 u^2(R_{\text{ac}}) + (K_4 C + R_{\text{ac}})^2 u^2(C)]. \tag{36}$$

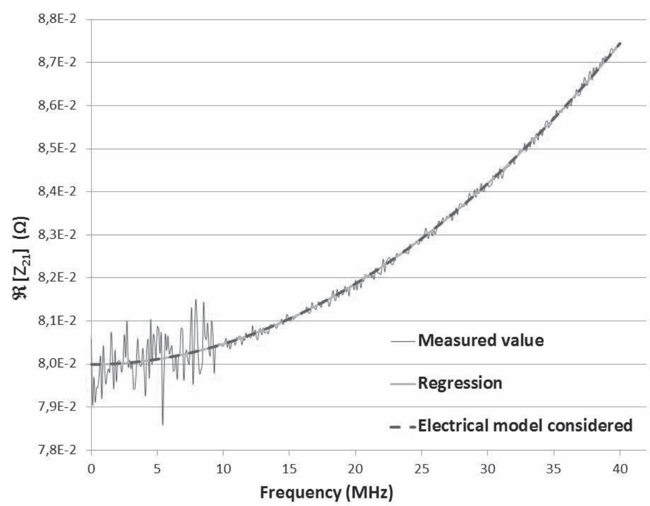

Fig. 4. Real part of the shunt based on a “cage” geometry of 10 A.

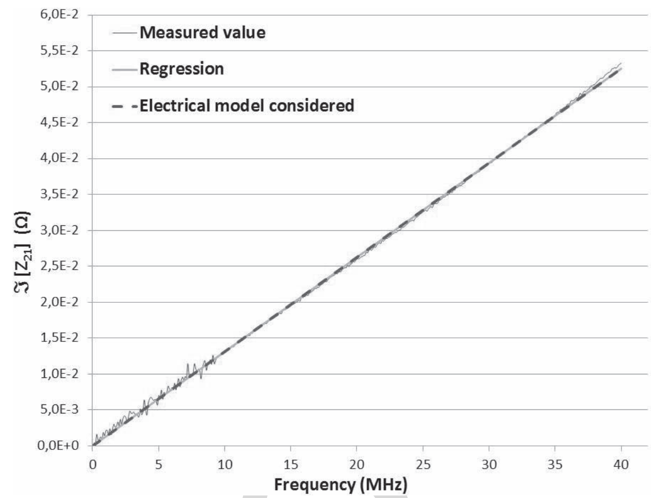

Fig. 5. Imaginary part of the shunt based on a “cage” geometry of 10 A.

V. Experimental Results

AC coaxial shunts based on the “cage” geometry (resistors in parallel within a cage structure) of 10 A and current shunts based on metal electrode leadless face (MELF) resistors from 0.5 up to 10 A have been measured. For clarity of this paper, only the results for a shunt of 10 A obtained are presented and compared to the existing methods in order to validate the approach proposed. It is important to note that comparable results are obtained for other current shunt values.

A VNA E5071C has been calibrated with a calibration kit developed at LNE. The measurements of “cage” and “MELF” current shunts have been performed up to 40 and 60 MHz, respectively. The VNA measurement parameters are:

1) sufficient frequency points (801 points) with a linear distribution;
2) averaging of five measurements at each frequency;
3) intermediate frequency of the VNA receiver equal to 100 Hz.

The method described in this paper has been applied to obtain ac–dc difference and phase angle values and the associated uncertainties. To summarize the experimental approach

1) First, the shunt impedance Z_{21} is calculated from the S-parameters measured with a VNA.
2) Then, the regressed value of the impedance Z_{21} is determined using the values of the electrical model (*RL* or *RC* circuit) which are calculated through the regression approach.
3) Finally, the ac–dc difference and phase angle parameters and its associated uncertainties are calculated.

Figs. 4–7 show the real and imaginary parts measured by the shunt impedance, the regression curves, and the curves obtained from the electrical model considered (*RC* or *RL*). Examples illustrated in Figs. 4–7 concern the 10-A ac coaxial shunts based on “cage” geometry and “MELF” resistors. We can observe measurement noise due to the low value of the 10-A shunt under study which is far from the 50-Ω reference impedance of the VNA and due to the very varied range of S-parameters measured from 9 kHz to 60 MHz: typically, from a few 10^{-4}–10^{-3}. In addition, the noise level becomes abruptly higher below 10 MHz because of the VNA’s internal electronic architecture. (Couplers are different below

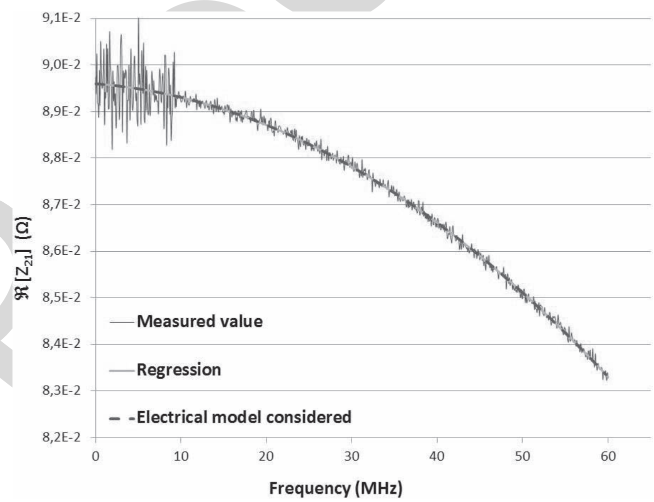

Fig. 6. Real part of the shunt based on “MELF” resistors of 10 A.

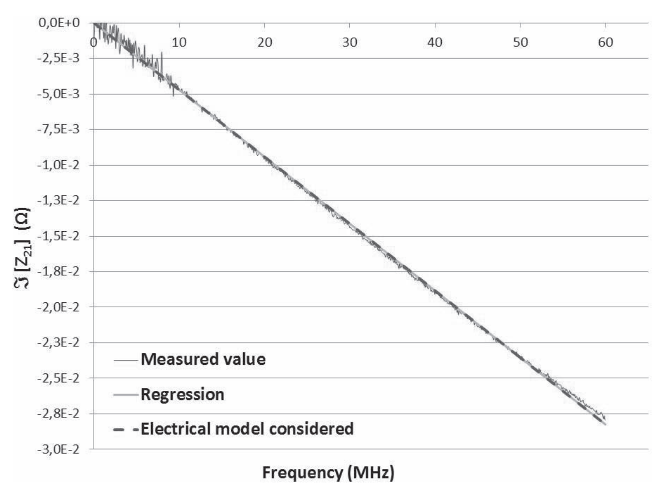

Fig. 7. Imaginary part of the shunt based on “MELF” resistors of 10 A.

TABLE I

CIRCUIT PARAMETERS OF THE MEASURED CURRENT SHUNTS

	DC Resistor value R_{DC} (mΩ)	Inductor value L (pH)	Capacitor value C (nF)
“cage” geometry of 10 A	79.99	209.05 ± 10.17	-
“MELF” resistors of 10 A	89.60	-	9.48 ± 1.11

TABLE II

AC–DC DIFFERENCE RESULTS OF THE AC COAXIAL SHUNT BASED ON A “CAGE” GEOMETRY OF 10 A WITH ITS EXPANDED UNCERTAINTIES AT 100 kHz

	VNA measurement	RISE laboratory measurement	Thermal transfer measurement by LNE
δ (μΩ/Ω)	3.8	62.0	45.5
u(δ) (μΩ/Ω)	199.3	135.0	86.0

TABLE III

PHASE ANGLE RESULTS OF THE AC COAXIAL SHUNT BASED ON A “CAGE” GEOMETRY OF 10 A WITH ITS EXPANDED UNCERTAINTIES AT 100 kHz

	VNA measurement	NMIA laboratory measurement
ϕ (μrad)	1642.0*	1000*
u(ϕ) (μrad)	146.2	124.0

* Values reported in this table concern shunts based on “cage” geometry but manufacturers are different. The shunts measured by NMIA laboratory and using the VNA method are not fabricated on the same design. Phase angle results should be considered as indicative values.

TABLE IV

AC–DC DIFFERENCE RESULTS OF THE CURRENT SHUNT BASED ON MELF RESISTORS OF 10 A WITH ITS EXPANDED UNCERTAINTIES AT 100 kHz

	VNA measurement	JV laboratory measurement	PTB laboratory measurement
δ (μΩ/Ω)	-15.7	-2.0	-18.0
u(δ) (μΩ/Ω)	160.43	11.0	70.0

TABLE V

PHASE ANGLE RESULTS OF THE CURRENT SHUNT BASED ON MELF RESISTORS OF 10 A WITH ITS EXPANDED UNCERTAINTIES AT 100 KHZ

	VNA measurement
ϕ (μrad)	-525.4
u(ϕ) (μrad)	105.0

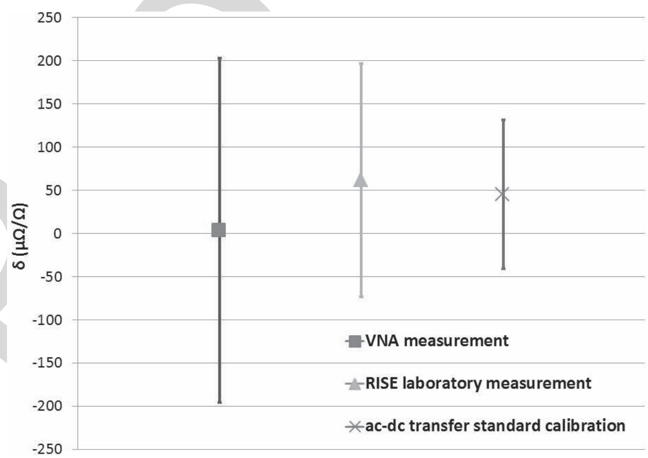

Fig. 8. AC–DC difference results of the current shunt based on a “cage” geometry of 10 A with its expanded at 100 kHz.

and above 10 MHz.) The polynomial regression applied in the presented method allows overcoming the measurement issue related to the noise observed. The curves of the imaginary parts measured are linear and, respectively, negative for shunts based on the “MELF” geometry and positive for shunts based on the “cage” resistor which corresponds to a capacitive and inductive behavior as expected. The real parts are quadratic for both the shunts that can be explained by losses in metallic parts and by the first resonance frequency which is below 300 MHz for both the shunts. Because the frequency resonance is close to the frequency bandwidth used for the polynomial regression, it is noted that the skin effect cannot be quantified from the VNA measurements since there is a combination of resonance and skin effect.

The values of R_{dc}, L, and C calculated are summarized in Table I. The results of ac–dc difference and phase angle parameters and the associated expanded uncertainties ($k = 2$) are presented in Tables II–V. At 100 kHz, the values are higher than those provided by the existing methods. Nevertheless, to our knowledge, the method presented in this paper is the only one able to perform in one step a broadband and simultaneous measurement of the magnitude and phase of current shunts up to a few megahertz with acceptable uncertainties. The measurement method used by the JV and PTB laboratories is a thermal transfer method [24], whereas the RISE laboratory uses a direct comparison method and the NMIA laboratory uses a potentiometer method [9]. The comparison of the ac–dc difference results is shown in Figs. 8 and 9. The results obtained with the VNA method is in very good agreement with the existing methods, particularly for the ac difference results of the current shunt based on “MELF” resistors: the difference of the mean values is significantly less than the uncertainty of the VNA method.

For the existing methods, the shunt parameters are obtained from the electrical current measurement values provided by a reference device. These methods are not able to provide simultaneously both parameters: ac–dc difference and phase angle. Moreover, these methods are mainly limited by the generation of a nominal current at high frequencies. Therefore, uncertainties on ac–dc difference and phase angle parameters depend on the uncertainties related to the high current levels to be produced for the measurements. This constraint explains the limitation of these methods to the low-frequency range (below 100 kHz).

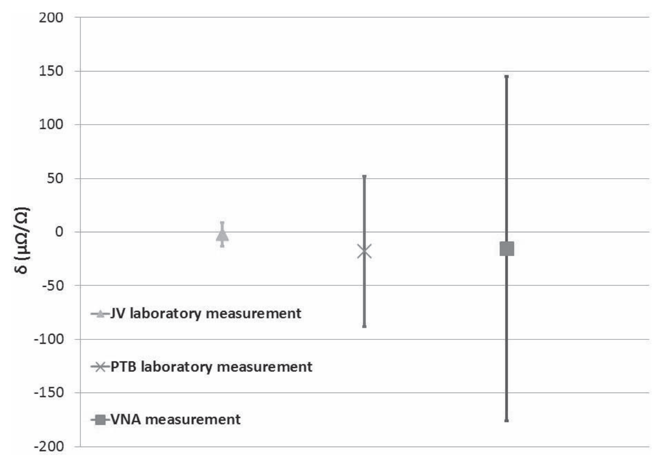

Fig. 9. AC–DC difference results of the current shunt based on MELF resistors of 10 A with its expanded uncertainty at 100 kHz.

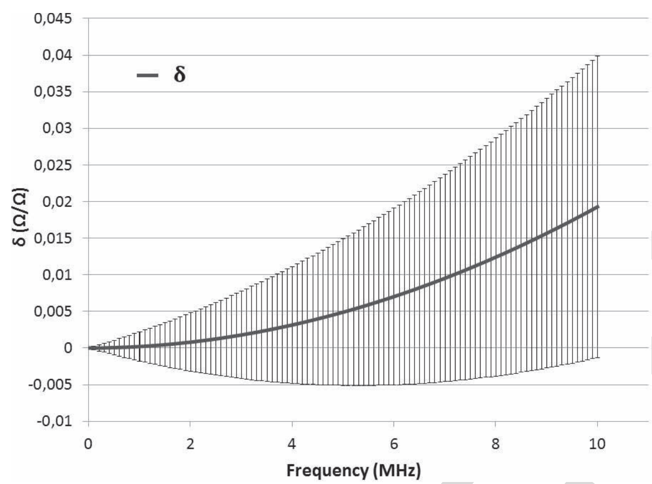

Fig. 10. AC–DC difference with its uncertainties of the ac coaxial shunt based on a “cage” geometry of 10 A up to 10 MHz.

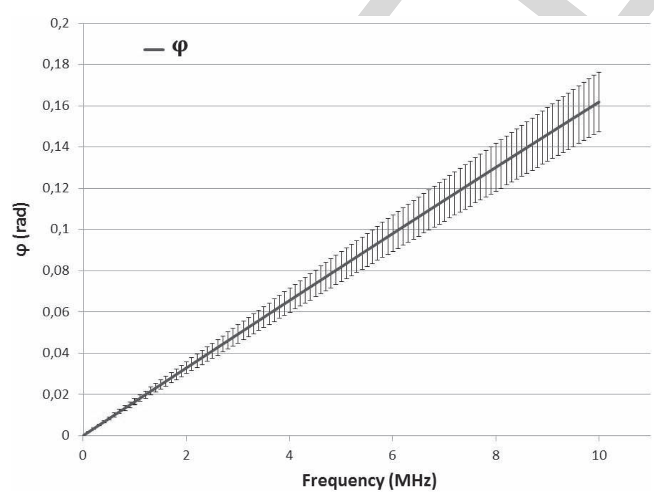

Fig. 11. Phase angle with its uncertainties of the ac coaxial shunt based on a “cage” geometry of 10 A up to 10 MHz.

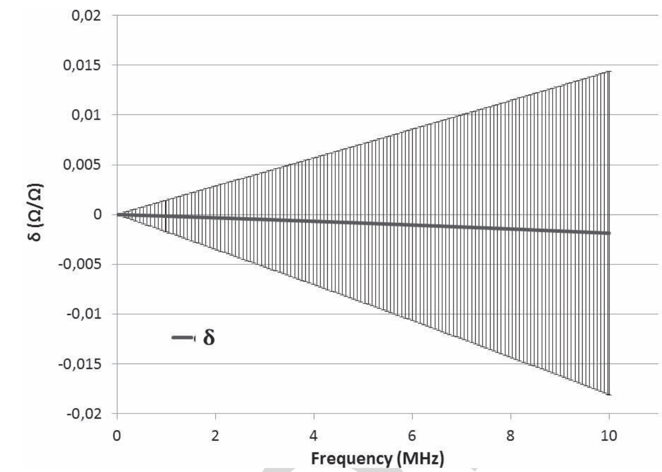

Fig. 12. AC–DC difference with its uncertainties of the current shunt based on MELF resistors of 10 A up to 10 MHz.

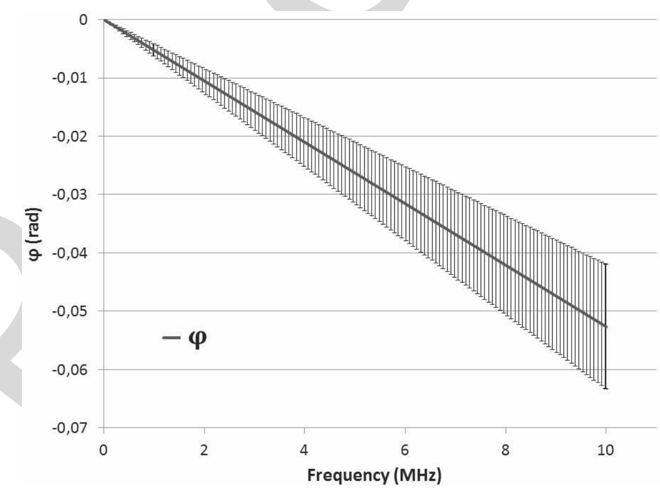

Fig. 13. Phase angle with its uncertainties of the current shunt based on “MELF” resistors of 10 A up to 10 MHz.

The proposed method extends the limiting frequency up to a few megahertz. Type A (reproducibility and repeatability intermediate precision conditions of measurement) and type B uncertainty contributions have been carefully taken into account in the S-parameters uncertainty evaluation. It is important to note that uncertainties of ac–dc difference and phase angle parameters are related to the impedance value of shunt. They are proportional to the inverse of the shunt resistance value [see (20), (22), (33)]. The method described in this paper allows determining simultaneously both the relevant parameters: ac–dc difference and phase angle. The current shunts frequency variation and the associated uncertainties are shown in Figs. 10–13. It can be observed that the frequency resonance impacts more strongly the ac–dc difference results in the case of the shunt based on the “cage” geometry.

VI. Conclusion

This paper has presented a new method for measuring and characterizing the standard current shunt up to a few megahertz. This method is based on the use of a VNA. The results of measurements presented in this paper illustrate the effectiveness of this method. Compared with the existing measurement methods, the one proposed has the advantage of increasing the measurement frequency beyond 100 kHz.

Furthermore, it allows to simultaneously measure the ac–dc difference and the phase angle error, which was until now impossible for current levels above 1 A. This method can be applied for current shunts for which a simple equivalent electrical model can be established with a temperature-independent frequency variation and a negligible skin effect on the shunt reactive part in the frequency range of interest. The obtained uncertainty levels are higher to those provided by the existing methods at 100 kHz, but to our knowledge, this new approach is the only one capable of measuring high current shunts in the megahertz frequency range. The Monte Carlo method has been implemented and results compared to the classical GUM approach to validate that the nonlinearity of measurement functions do not impact uncertainties evaluated by the classical GUM method. It is noted that the impact of the nonlinearity on the combined uncertainties depends on the standard deviations of input variables. For instance, if standard deviations are low enough, the nonlinearity can be negligible and the higher orders of the Taylor expansion have not to be considered. If the input variables (S-parameters) of the presented method have too higher standard deviations, the nonlinearity effect should be considered to calculate uncertainties following the classical GUM method or the Monte Carlo method should be applied in this case.

REFERENCES

[1] K.-E. Rydler, T. Bergsten, and V. Tarasso, "Determination of phase angle errors of current shunts for wideband power measurement," in *Proc. Conf. Precis. Electromagn. Meas.*, Jul. 2012, pp. 284–285.

[2] *The BIPM Key Comparison Database*. accessed: Apr. 2018. [Online]. Available: http://kcdb.bipm.org/

[3] J. R. Kinard, T. E. Lipe, and C. B. Childers, "AC-DC difference relationships for current shunt and thermal converter combinations," in *Proc. Conf. Precis. Electromagn. Meas.*, Jun. 1990, pp. 136–137.

[4] S. Svensson, K.-E. Rydler, and V. Tarasso, "Improved model and phase-angle verification of current shunts for AC and power measurements," in *Proc. Conf. Precis. Electromagn. Meas.*, Jun./Jul. 2004, pp. 82–83.

[5] U. Pogliano, B. Trinchera, and D. Serazio, "Wideband digital phase comparator for high current shunts," *Metrologia*, vol. 49, no. 3, p. 349, 2012.

[6] G. C. Bosco *et al.*, "Phase comparison of high-current shunts up to 100 kHz," *IEEE Trans. Instrum. Meas.*, vol. 60, no. 7, pp. 2359–2365, Jul. 2011.

[7] X. Pan *et al.*, "Measurement of the phase angle errors of high current shunts at frequencies up to 100 kHz," *IEEE Trans. Instrum. Meas.*, vol. 62, no. 6, pp. 1652–1657, Jun. 2013.

[8] B. Pinter, M. Lindič, B. Voljč, Z. Svetik, and R. Lapuh, "Modeling of AC/DC current shunts," in *Proc. CPEM*, Jun. 2010, pp. 599–600.

[9] I. Budovsky, "Measurement of phase angle errors of precision current shunts in the frequency range from 40 Hz to 200 kHz," *IEEE Trans. Instrum. Meas.*, vol. 56, no. 2, pp. 284–288, Apr. 2007.

[10] K.-E. Rydler and V. Tarasso, "A method to determine the phase angle errors of an impedance meter," in *Proc. Conf. Precis. Electromagn. Meas.*, Jun./Jul. 2004, pp. 123–124.

[11] K.-E. Rydler, "High precision automated measuring system for AC-DC current transfer standards," *IEEE Trans. Instrum. Meas.*, vol. 42, no. 2, pp. 608–611, Apr. 1993.

[12] A. Mortara and F. Pythoud, "Wideband accurate calibration of a current probe," in *Proc. Conf. Precis. Electromagn. Meas.*, Jul. 2012, pp. 484–485.

[13] K. Lind, T. Sørsdal, and H. Slinde, "Design, modeling, and verification of high-performance AC–DC current shunts from inexpensive components," *IEEE Trans. Instrum. Meas.*, vol. 57, no. 1, pp. 176–181, Jan. 2008.

[14] L. Scarioni, M. Klonz, and T. Funck, "Quartz planar multijunction thermal converter as a new AC-DC current transfer standard up to 1 MHz," in *Proc. Conf. Precis. Electromagn. Meas.*, Jun./Jul. 2004, pp. 455–456.

[15] D. Fortuné, D. Istrate, F. Ziadé, and I. Blanc, "Measurement method of AC current up to 1 MHz," Tech. Rep., Jan. 2014, pp. 35–39.

[16] F. Ziade, A. Poletaeff, and D. Allal, "Primary standard for S-parameter measurements at intermediate frequencies (IFs)," *IEEE Trans. Instrum. Meas.*, vol. 62, no. 3, pp. 659–666, Mar. 2013.

[17] I. Budovsky, A. M. Gibbes, and D. C. Arthur, "A high-frequency thermal power comparator," *IEEE Trans. Instrum. Meas.*, vol. 48, no. 2, pp. 427–430, Apr. 1999.

[18] *Agilent Network Analyzer Basics*. accessed: Dec. 2017. [Online]. Available: http://www.agilent.com/home

[19] A. Ferrero and U. Pisani, "Two-port network analyzer calibration using an unknown 'thru,'" *IEEE Microw. Guided Wave Lett.*, vol. 2, no. 12, pp. 505–507, Dec. 1992.

[20] D. M. Pozar, *Microwave Engineering*, 4th ed. Hoboken, NJ, USA: Wiley, 2011.

[21] *Evaluation of Measurement Data—Guide to the Expression of Uncertainty in Measurement*, document JCGM 100:2008, BIPM, 2008.

[22] *Evaluation of Measurement Data—Supplement 1 to the 'Guide to the Expression of Uncertainty in Measurement'—Propagation of Distributions Using a Monte Carlo Method*, document JCGM 101, BIPM, 2008.

[23] *The BIPM Key Comparison Database, Calibration and Measurement Capabilities Electricity and Magnetism*, Jan. 2015.

[24] H. Malmbekk, "Final report: EURAMET.EM-S39," *Metrologia*, vol. 52, no. 1A, p. 01003, 2015.

Mohamed Ouameur was born in Ouarzazate, Morocco, in 1990. He received the M.Sc. degree in electrical engineering from Polytech Clermont-Ferrand, Aubière, France, in 2014. He is currently pursuing the Ph.D. degree with the Laboratoire National de Métrologie et d'Essais, Trappes, France.

He was with the Geeps, Laboratoire de Génie Electrique de Paris, Centrale Supélec, CNRS, Université Paris-Sud, Université Paris-Saclay, Gif-sur-Yvettes, France. His current research interests include the traceability of electrical current measurement up to 1 MHz and 10 A.

François Ziade was born in Tremblay-en-France, France, in 1979. He received the M.Sc. degree in applied physics, electronics, and microwave engineering from the University of Pierre et Marie Curie, Paris, France, in 2003, and the Ph.D. degree in electronics and telecommunications from Telecom ParisTech, Paris, in 2008, with a focus on power standards.

In 2007, he joined the Laboratoire National de Métrologie et d'Essais, Trappes, France, as a Researcher. His current research interests include establishing impedance traceability at lower RF, EMC measurements, S-parameters, and terahertz measurements.

Yann Le Bihan received the Ph.D. degree from ENS de Cachan, Cachan, France, in 2000, and the Enabling Degree to supervise Ph.D. Studies (HDR) of Université Paris-Sud, Orsay, France, in 2007.

He was a Former Student with the Aggregation of Electrical Engineering, ENS de Cachan, in 1996. In 2000, he joined the Laboratoire de Génie Electrique de Paris. From 2001 to 2011, he was an Assistant Professor at the IUT de Cachan, Université Paris-Sud, where he has been a Professor since 2011. His current research interests include characterization and nondestructive testing by electromagnetic methods: modeling, sensor design, and inverse problems.